

8-1-2005

Measurements of Secondary Organic Aerosol from Oxidation of Cycloalkenes, Terpenes, and m-Xylene Using an Aerodyne Aerosol Mass Spectrometer

Roya Bahreini

California Institute of Technology

Melita D. Keywood

California Institute of Technology

Nga L. Ng

California Institute of Technology

Varuntida Varutbangkul

California Institute of Technology

Song Gao

California Institute of Technology, sg1002@nova.edu

See next page for additional authors

Follow this and additional works at: https://nsuworks.nova.edu/cnso_chemphys_facarticles

 Part of the [Environmental Chemistry Commons](#)

NSUWorks Citation

Bahreini, R., Keywood, M. D., Ng, N. L., Varutbangkul, V., Gao, S., Flagan, R. C., Seinfeld, J. H., Worsnop, D. R., & Jimenez, J. L. (2005). Measurements of Secondary Organic Aerosol from Oxidation of Cycloalkenes, Terpenes, and m-Xylene Using an Aerodyne Aerosol Mass Spectrometer. *Environmental Science & Technology*, 39, (15), 5674 - 5688. <https://doi.org/10.1021/es048061a>. Retrieved from https://nsuworks.nova.edu/cnso_chemphys_facarticles/151

This Article is brought to you for free and open access by the Department of Chemistry and Physics at NSUWorks. It has been accepted for inclusion in Chemistry and Physics Faculty Articles by an authorized administrator of NSUWorks. For more information, please contact nsuworks@nova.edu.

Authors

Roya Bahreini, Melita D. Keywood, Nga L. Ng, Varuntida Varutbangkul, Song Gao, Richard C. Flagan, John H. Seinfeld, D. R. Worsnop, and J. L. Jimenez

Chapter 10
Measurements of Secondary Organic Aerosol (SOA) from
Oxidation of Cycloalkenes, Terpenes, and *m*-xylene using an
Aerodyne Aerosol Mass Spectrometer*

* This chapter is reproduced with permission from “Measurements of Secondary Organic Aerosol (SOA) from oxidation of cycloalkenes, terpenes, and *m*-xylene using an Aerodyne Aerosol Mass Spectrometer” by R. Bahreini, M.D. Keywood, N.L. Ng, V. Varutbangkul, S. Gao, R.C. Flagan, J.H. Seinfeld, D.R. Worsnop, and J.L. Jimenez, *Environ. Sci. Tech.*, submitted for publication, unpublished work copyright 2004, American Chemical Society.

10.1. Abstract

The Aerodyne Aerosol Mass Spectrometer (AMS) was used to characterize physical and chemical properties of secondary organic aerosol (SOA) formed during ozonolysis of cycloalkenes and biogenic hydrocarbons and photooxidation of *m*-xylene. Comparison of mass and volume distributions from the AMS and Differential Mobility Analyzers yielded estimates of “effective” density of the SOA in the range of 0.64-1.45 g/cm³, depending on the particular system. Increased contribution of the fragment at *m/z* 44, CO₂⁺ ion fragment of oxygenated organics, and higher “delta” values, based on ion series analysis of the mass spectra, in nucleation experiments of cycloalkenes suggest greater contribution of more oxygenated molecules to the SOA compared to those formed under seeded experiments. Dominant negative “delta” values of SOA formed during ozonolysis of biogenics indicates presence of terpene derivative structures or cyclic or unsaturated oxygenated compounds in the SOA. Evidence of acid-catalyzed heterogeneous chemistry, characterized by greater contribution of higher molecular weight fragments to the SOA and corresponding changes in “delta” patterns, is observed in the ozonolysis of α -pinene. Mass spectra of SOA formed during photooxidation of *m*-xylene exhibit features consistent with the presence of furandione compounds and nitro organics. This study demonstrates that mixtures of SOA compounds produced from similar precursors result in broadly similar AMS mass spectra. Thus, fragmentation patterns observed for biogenic vs. anthropogenic SOA may be useful in determining the sources of ambient SOA.

10.2. Introduction

Secondary organic aerosols (SOA) are a significant contributor to the total ambient organic aerosol loading in urban areas, as well as regionally and globally. Our understanding of SOA formation processes and their chemical and physical properties is, however, limited. Better understanding of SOA is essential in order to accurately evaluate the impact of SOA on visibility, climate, and human health and to incorporate this understanding in future regulations. Traditionally, controlled laboratory chamber experiments have been carried out to determine the SOA forming potential, i.e., organic yield, of volatile hydrocarbons that are, or have a chemical structure close to, atmospherically relevant compounds (*1-6*).

Laboratory chamber experiments have been instrumental in identifying specific compounds formed as SOA. Recent studies have demonstrated the presence of polymeric structures in the SOA formed from both anthropogenic and biogenic hydrocarbon precursors (*7-11*). Formation of such polymeric structures has been suggested to occur by aerosol-phase reactions, possibly acid-catalyzed, such as aldol condensation, gem-diol reaction, and hemiacetal/acetal formation pathways (*12*). Oligomers have been identified in the SOA formed in both the presence and absence of inorganic acids (*7,9*).

The Aerodyne Aerosol Mass Spectrometer (hereafter referred to as the AMS) provides mass concentration and mass size distribution of non-refractory components of sub-micron aerosols in real time (*13,14*). Because of the high time and size resolution of the data collected by the AMS, the AMS has been deployed in many field studies, both airborne and ground-based, measuring size-resolved chemical composition of ambient aerosols (*14-19*). The AMS has also been used in laboratory-chamber studies (*20-22*).

The current work summarizes studies of laboratory-chamber generated SOA using the AMS. A comprehensive series of experiments was conducted to study ozonolysis of cycloalkenes and biogenic precursors to investigate SOA physical and chemical characteristics and effect of heterogeneous reactions on SOA formation. In addition, photooxidation of *m*-xylene, a predominant SOA-forming anthropogenic hydrocarbon, was studied. Experiments were carried out in the absence or presence of seed particles of varying composition. Figure 10.1 gives the chemical structures of the precursors studied.

In order to compute a mass yield of SOA, it is necessary to know the SOA density since the volumetric yield is the quantity normally determined in chamber experiments. Estimates of the density of SOA have so far been based on the detailed chemical speciation of the SOA. Because it has been traditionally difficult to identify the complete composition of SOA, the estimated density is uncertain because of the missing contribution of unidentified products. It is demonstrated in the current study that SOA effective density can be estimated by comparing mobility volume distributions with AMS mass distributions measured in parallel. The work presented here demonstrates that information on types of organics present, degree of contribution of higher molecular weight species (or those with higher resistance to fragmentation) to the SOA, and indications of types of SOA precursors can be obtained in the analysis of the AMS organic mass spectra. Because of these specific characteristics observed in the mass spectra, it is then possible to extend the analysis to ambient data where analogies are drawn from patterns observed during laboratory chamber experiments in order to explore the potential contributions of various precursor classes to the formation of the ambient SOA.

10.3. Experimental

Experiments were conducted in Caltech's indoor dual 28 m³ suspended FEP Teflon chambers (23). The AMS was used to measure size-resolved aerosol chemical composition. A complete description of the AMS and its data analysis is given elsewhere (13,14,24,25). In summary, sample (gas and particle phase) is introduced into the differentially pumped chambers of the instrument through a 100 μm critical orifice. An aerodynamic lens system is used to collimate the particles into a narrow beam. A chopper wheel (~2% duty cycle) is used to chop the particle beam for "time of flight" mode measurements (i.e., P-TOF mass distribution measurements) or to block/clear the particle beam for "mass spectrum" mode measurements (MS). Upon impacting on the vaporizer (~650 °C), which is positioned at the end of the P-TOF chamber, the non-refractory components in/on the aerosols are vaporized, and the vapors are ionized under high vacuum by electron impact (70 eV). Positive ions are then extracted into the quadrupole mass spectrometer for determination of their mass-to-charge ratio (m/z).

The particle size calibration of the AMS was determined by sampling dry polystyrene latex (PSL) particles (Duke Scientific) and validated using DMA size-selected dry ammonium nitrate and/or ammonium sulfate particles. Ionization efficiency calibration of the AMS, needed to determine the mass concentration of species from raw MS ion signals, was performed on a regular basis by sampling DMA size-selected dry ammonium nitrate particles. Further details of these calibrations and the relevant calculations can be found elsewhere (14,24).

Aerosol size distributions, in the size range of ~15-775 nm in mobility diameter, were measured by scanning electrical mobility spectrometers (SEMS) (26). Each SEMS

system includes a ^{85}Kr neutralizer (TSI model 3077), a long cylindrical column differential mobility analyzer (DMA, TSI model 3081), and a condensation particle counter (CPC, TSI model 3760). The flow rates of the SEMS systems are controlled to 2.5 LPM for sheath and excess flows and 0.25 LPM for polydisperse and monodisperse aerosol flows. In addition, the total number concentration of particles in each chamber was measured by additional CPCs (TSI, models 3010 and 3025). A hygroscopic tandem differential mobility analyzer (HTDMA) was used in a number of experiments to determine the hygroscopic behavior of the SOA. Furthermore, bulk filter samples were collected for organic speciation analysis (9,11).

Gas-phase concentrations of parent hydrocarbons were measured by a gas chromatograph with a flame ionization detector (GC-FID, Hewlett Packard model 5890, series II Plus). Ozone concentration was measured by a Horiba ambient O_3 monitor (model APOA-360 CE), and concentrations of nitrogen oxides were measured by a Horiba ambient $\text{NO-NO}_2\text{-NO}_x$ monitor (model APNA-360). Temperature and humidity of the chamber were also measured by Vaisala probes (HMP230 series transmitters). Details on calibration procedures of the above instruments are given elsewhere (6).

During seeded experiments, seed particles were generated by atomizing salt-water solutions using a constant rate atomizer. Non-acidic bulk solutions were made at 0.03 M concentration of the salt (ammonium sulfate or magnesium sulfate); acidic bulk solutions were made of 0.03 M concentration of the salt (ammonium sulfate or magnesium sulfate) and 0.05 M or 0.1 M of sulfuric acid. Since the atomized particles are highly charged, they were passed through ^{210}Po neutralizers in order to achieve a more neutral charge distribution and reduce particle loss in the lines. In low relative humidity experiments,

particles were also passed through a silica-gel diffusion drier before being introduced into the chamber.

The temperature in the chambers was maintained at 20 ± 2 °C. Relative humidity of the chamber was controlled by controlling the humidity of the flushing air. For dry experiments, chambers were flushed with dry-scrubbed air with RH < 10%. For humid experiments, dry-scrubbed air was passed through a bubbler and a particle filter before being introduced into the chamber at a rate such that the relative humidity achieved in the chamber at 20 °C was $\sim 55 \pm 5$ %. During photooxidation studies, 300, 40 W each, 350-BL lights were used to illuminate the chambers (23).

Volatile hydrocarbons (Sigma Aldrich) were introduced as liquid samples into injection glass bulbs. The liquid was then heated gently in the bulb, and the vapors were carried to the chamber by passing scrubbed air through the bulb. During dark ozonolysis experiments, cyclohexane, used as the hydroxyl radical (OH) scavenger, was introduced into the chamber in a similar manner. The role of different OH scavengers in ozonolysis experiments, in terms of producing additional HO₂ and RO₂ radicals that may change the ozonolysis chemistry of alkenes or terpenes, has been the subject of previous studies. Keywood *et. al.* (27) reported that the SOA yield during cyclohexene ozonolysis was 30% lower in the presence of cyclohexane as opposed to 2-butanol as the scavenger. However, Docherty and Ziemann (28) reported that the SOA yield during β-pinene ozonolysis was 3 times higher in the presence of cyclohexane as opposed to propanol as the scavenger. Based on these recent studies, it is apparent that the extent by which the scavenger affects the radical chemistry during ozonolysis experiments depends on the structure of the specific compound being studied. For consistency, however, only

cyclohexane was used as the scavenger during the experiments from which we report results. The concentration of cyclohexane injected for each experiment was based on the concentration of the parent hydrocarbon and reaction rates of the parent hydrocarbon and cyclohexane with OH radical such that 99% of the time cyclohexane, rather than the parent hydrocarbon, would react with the OH radical.

During photooxidation studies, NO (502 ppm in nitrogen, Scott-Marrin Inc.), NO₂ (521 ppm in nitrogen, Air Liquide), and propene (500 ppm in nitrogen, Air Liquide) were injected into the chamber.

Concentrations of the parent hydrocarbon and the seed- in the case of seeded experiments- or NO_x levels- in the case of photooxidation experiments- were monitored for at least 1 h to ensure stability of the system before start of the reaction. Start of the reaction in ozonolysis studies was marked by ozone injection using a UV lamp ozone generator (EnMet Corporation). Ozone injection continued until the concentration of ozone exceeded by a factor of two or three the initial hydrocarbon concentration, depending on the experiment, to ensure full oxidation. During photooxidation experiments, turning on the chamber's UV source lamps marked the beginning of the reaction.

10.4. Determination of SOA Density and Morphology

As stated above, an estimate of density is needed to convert an apparent volume measurement of SOA into mass concentration, such as in SOA yield calculations using DMA measurements of size distribution. Without all the significant components of the SOA being identified, the estimation of the density based on the chemical composition may be subject to biases if a class of compounds with different density goes

systematically undetected. Comparing parallel AMS mass distribution measurements and DMA volume distributions provides an estimate of aerosol effective density (21,29,30). The AMS mass distribution is measured vs. vacuum aerodynamic diameter (d_{va}) whereas DMA volume distribution is measured vs. electrical mobility diameter (d_m). The vacuum aerodynamic diameter is the diameter of a sphere, in the free molecular regime, with unit density (1 g/cm^3) and the same terminal velocity as the particle of interest. The mobility diameter is the diameter of a sphere with the same migration velocity of the particle of interest in a constant electric field at atmospheric pressure. These two measures of particle size are related by “effective density” (ρ_{eff}) or “material density” (ρ_m) as follows:

$$\rho_{eff} = \frac{d_{va}}{d_m} \rho_0 = \rho_m \frac{C_c(d_{ve})}{\delta^3 \chi_t \chi_v C_c(d_m)} \quad (1)$$

where ρ_0 is unit density (1 g cm^{-3}), C_c is the Cunningham slip correction factor, d_{ve} is the volume equivalent diameter, δ is the internal void fraction, χ_t is the dynamic shape factor in the transition regime, and χ_v is the dynamic shape factor in the free molecular regime (30). Note that several other definitions of effective densities are used in the literature; these definitions are equivalent for spherical particles but can be significantly different when particles are irregular (30). When comparing AMS and DMA aerosol mass distributions in order to deduce the SOA density, only the rising edge of the small-size bins of the distributions was considered for the following reasons: (1) transmission efficiency in the AMS is 100% for 100-500 nm particles (P. Liu, University of Wyoming, unpublished data) (13), which is also the size range of interest; (2) during some experiments, a longer tail on the AMS mass distributions was observed, which can be an artifact of slower evaporation of some components of the aerosols; (3) during some

nucleation experiments, nucleated particles grew to sizes larger than the scan-range of the DMA, thus limiting the comparison only to smaller sizes. As shown in Figures 10.2a-10.2b, this comparison has been proven successful to better than $\pm 10\%$ for ammonium nitrate and ammonium sulfate aerosols. During seeded experiments, the estimates of ρ_{eff} and mass concentration measurements of the seed and SOA (m_{seed} and m_{SOA}) were used along with the assumption of unit dynamic shape factor ($\chi = 1$, i.e., particle sphericity) to determine density of SOA (ρ_{SOA}) based on the following relationship which also assumes volume additivity:

$$\rho_{eff} = \frac{m_{seed} + m_{SOA}}{V_{seed} + V_{SOA}} = \frac{m_{seed} + m_{SOA}}{\frac{m_{seed}}{\rho_{seed}} + \frac{m_{SOA}}{\rho_{SOA}}} \quad (2)$$

Typical evolution of the SOA concentration and mass distribution during an experiment is shown in Figures 10.3a-10.3c; condensation of secondary organics onto the seed causes a shift in the mass distribution of the seed and SOA to larger sizes. During this growth, the width of the mass distribution decreases, indicating condensation is the main mechanism of growth. Although particle loss to the chamber walls is also expected to narrow the mass distribution, analysis of mass distributions obtained during “wall-loss experiments”, where the loss rate of the seed particles to the chamber walls is characterized, indicates that the width of the distributions does not change appreciably for durations typical of SOA experiments.

Information about morphology of the aerosols can be deduced by comparing the sulfate signal before and after start of the reaction during seeded experiments.

Unpublished data from our laboratory experiments have shown collection efficiency of only $\sim 30\%$ in the AMS for dry ammonium sulfate particles, most likely due to bounce of

dry and less volatile particles off of the AMS vaporizer (T. Onasch, Aerodyne Research, Inc., personal communication). It has been observed that collection efficiency of ambient particles increases once the AMS inlet temperature approaches the ambient dew point and particles deliquesce and become liquid droplets (16). A similar phenomenon is observed here as SOA condenses on the seed aerosol during the first stages of the reaction. Figure 10.4 shows the time trend of mass concentration of sulfate and organics for cyclopentene ozonolysis; the sulfate signal increases by a factor of ~ 2 once ozone injection, and consequently SOA formation starts. As discussed subsequently, this phenomenon was not observed with oxidation of all hydrocarbons, which suggests different particle phases (liquid vs. solid) within the AMS vacuum conditions for the SOA formed from different precursors.

10.5. Analysis of Organics

As gas-phase organics partition into the aerosol phase, different organic peaks appear in the AMS mass spectra (Figure 10.3d-10.3e). The ion series (or “delta (Δ)”) analysis technique was developed in an attempt to characterize chemical properties and specific features of the EI mass spectra of classes of organic compounds (31). Because of the combination of high-temperature vaporization (650 °C) and relatively hard ionization of molecules in the AMS (electron impact ionization, 70 eV), individual compounds undergo significant fragmentation. Through ion series analysis, it is possible to obtain semi-quantitative information about the classes of compounds present in a mixture of organic compounds such as the SOA aerosols studied here. In this analysis, organic compounds are assumed to contain one or several functional groups and saturated and unsaturated hydrocarbon chains. Upon electron impact ionization, the hydrocarbon chain

can fragment at different positions, giving rise to mass spectra in which groups of peaks are separated by 14 amu units (for saturated chains). The m/z 's measured for a given compound are an indication of the functional groups in the molecule. A delta value ($\Delta = m/z - 14n + 1$, where n is the "nominal" number of CH_2 groups left on the functional group) is calculated for each m/z , which is an indication of the functionality of the fragment. For example, it is observed that unsaturated organics and aromatics yield Δ values ≤ 0 while oxygenated organics yield Δ values ≥ 2 (31). Although more details will be discussed subsequently, it is worth noting that the SOA generated by the various systems studied here show very different characteristics based on ion series analysis. The patterns determined in chamber experiments can be used in interpreting mass spectra obtained by AMS from ambient aerosols and help provide a better understanding of the main precursors of ambient SOA.

10.6. Results and Discussion

10.6.1. Dark Ozonolysis of Cycloalkene Precursors

A series of experiments with C_5 - C_8 cycloalkenes was conducted in order to investigate the effect of the parent hydrocarbon structure, such as position of the double bond or a methyl substituent, on SOA yield and other physical and chemical properties of SOA (6). These experiments were conducted in the presence of ammonium sulfate seed as well as in the absence of any seed.

As depicted as an example in Figure 10.4, during all cycloalkene experiments, the sulfate signal of the seed increased after start of reaction, indicating that the particle collection efficiency had increased. This suggests that the SOA formed in cycloalkene ozonolysis is likely in liquid phase, and that the aerosols changed as a result of

condensation of SOA on the seed particles, such that the probability of bounce of organic-coated seed particles on the vaporizer decreased and thus collection efficiency increased.

The effective density of SOA was determined as described in Section 3 and is tabulated in Table 2. Since the organic phase appears to be liquid, it was assumed that the particles are spherical, and thus the effective density should be a good estimate of the true material density. On average, ρ_{SOA} was $1.10 \pm 0.04 \text{ g/cm}^3$ during seeded experiments in contrast to $1.39 \pm 0.05 \text{ g/cm}^3$ during nucleation experiments with similar precursor concentrations. The fact that density of the SOA formed during nucleation experiments is ~25% higher than that of SOA formed during seeded experiments may suggest that either the particles sampled during seeded experiments are not spherical or the chemistry leading to the presence of organics in the aerosol phase is different under the two systems, such that it leads to formation of denser organic species during nucleation experiments. As shown in Figure 10.5 as an example, the fragments that are dominant for oxygenated organics, mainly $C_nH_{2n-1}O_2^+$ fragments with $\Delta = 4$ and CO_2^+ fragment (m/z 44) from thermal decomposition of oxygenated organics on the AMS vaporizer, indeed contribute to a greater extent to the total SOA mass for nucleation-generated SOA of cycloheptene.

Consistent observations of increased ion signal intensities of organic acids in the SOA during nucleation experiments have also been made in the ozonolysis of α -pinene by ion trap mass spectrometry (electrospray ionization source, direct infusion injection of the SOA sample). Although this observation was made in a different system (ozonolysis of α -pinene rather than cycloalkenes), it is still consistent with the qualitative trends of the

AMS observations presented here. For example, it is seen in the negative-ion mode mass spectra in Figure 10.6 that ion signals at m/z 171, 185, and 199 (corresponding to norpinic acid, pinic acid, and hydroxy pinonic acid, respectively, and likely their isomers- all gas phase oxidation products) increase by 50%, 24%, and 130%, respectively, in the nucleation experiment (Figure 10.6b) compared to the non-acid seeded one (Figure 10.6a). It is also seen in Figure 10.6b that ion signal intensities of some oligomers (m/z 299, 357, and 399) increase by at least 25% in the nucleation experiment, which may explain in part its higher SOA yield compared to that in the non-acid seeded experiment (11).

There is a trend of increasing SOA effective density with increasing contribution of m/z 44 to the total organic signal in the oxidation of many of the hydrocarbon precursors studied here (Figure 10.7). Although it is not possible to rule out completely the possibility of shape effects on lower estimates of SOA effective density during seeded experiments, the AMS mass spectra provided the evidence that there is an increased contribution of more oxygenated organics, which are generally denser, to the total SOA during nucleation experiments.

During the course of the cycloalkene ozonolysis experiments, the specific features of the organic mass spectra did not exhibit much change in time, as shown in Figures 10.3d-10.3e, except for increase in absolute intensity of organic peaks relative to the sulfate peaks.

10.6.2. Dark Ozonolysis of Biogenic Precursors

SOA formation during ozonolysis of biogenic precursors, namely monoterpenes, sesquiterpenes, and oxygenated terpenes, was studied. The phase/morphology of the SOA

produced is such that the seed signal decreased after the start of condensation of organics, indicating less efficient collection of SOA-coated sulfate particles. One possible explanation is that the SOA formed during ozonolysis of biogenics is in solid-phase under the vacuum conditions of the AMS; therefore, there is a greater probability of bounce of these SOA-coated particles on the AMS vaporizer. For example, it is shown in Figure 10.8 that after start of condensation of SOA from ozonolysis of linalool, the sulfate signal of the seed decreased by ~26%, which cannot be explained only by particle loss to the walls.

The effective density of SOA formed from ozonolysis of biogenic hydrocarbons was calculated following the method outlined in Section 3. Since the particles are likely in solid phase within the AMS and potentially non-spherical, the estimated densities are a lower bound of the true material densities (30). On average, biogenically derived SOA have lower “effective” densities compared to the SOA formed from nucleation-oxidation of cycloalkenes (Table 3), which may be due to real differences in material density as well as shape effects.

The biogenic precursors studied here showed distinct characteristics in the ion series pattern when compared to those of cycloalkene and *m*-xylene SOA. Generally, fragments in different *m/z* ranges exhibit different patterns of delta values. Here, three categories with different fragment size, with the nominal ranges of C₁-C₄, C₅-C₆, and C₇-C₁₅, are considered since the delta patterns shift from fragments of C₁-C₄ category to those of C₇-C₁₅. As shown in Figure 10.9, the larger fragments of SOA from biogenic precursors show a sharp contrast to cycloalkene and *m*-xylene SOA in that these larger fragments have dominantly negative delta values. An exception to this observation is terpinolene;

however, the backbone of terpinolene molecule is more similar to that of a methylene-substituted cycloalkene. Thus, it is not surprising that the fragmentation pattern of SOA formed from terpinolene ozonolysis is closer to that of SOA formed from ozonolysis of cycloalkenes. Dominant negative delta values are indicative of organic molecules that are terpene derivatives or have unsaturated or cyclic oxygenated structures.

The bicyclic compounds studied here, namely α -pinene, β -pinene, and Δ^3 -carene, have similar average delta values for larger fragment sizes, as shown in Figure 10.9, due to the similarity in their structures. A quite different precursor studied was 4-allylanisole, the SOA from which exhibits a very dominant low Δ value in its fragmentation pattern. We conclude that the benzyl fragment (m/z 77, $\Delta = -6$) and $\text{CH}_3\text{OC}_6\text{H}_4\text{CH}_2^+$ fragment (m/z 121, $\Delta = -4$) are the dominant contributors to the low average Δ values. Among all the biogenic precursors studied here, the SOA formed from ozonolysis of linalool exhibits the smallest contribution of larger fragments to the total SOA mass (only 4.5% from C_7 - C_{15} fragments). Because of the chemical structure and position of the double bonds in linalool, it is suspected that the primary ozonolysis products of linalool are only small-oxygenated molecules that only partition into the aerosol phase to a small extent. This hypothesis is further supported by low SOA yield observed for linalool. It is also interesting to note that the SOA formed from linalool yielded the lowest estimate of effective density of all systems studied, which may suggest the growth of somewhat non-spherical or porous particles. During the oxidation of biogenic precursors that have similar molecular weight and similar structures, namely α -pinene, Δ^3 -carene, α -terpinene, and terpinolene, it was observed that the organic yield was proportional to the mass fraction of larger organic fragments (C_5 - C_{15}). This is an indication that the SOA systems

that have greater organic yields also contain greater amounts of larger organic molecules, and possibly have a higher contribution of oligomeric structures (or of molecules that are more resistant to fragmentation) to the total SOA mass.

It is suspected that the reactions leading to formation of higher molecular weight SOA species are catalyzed in the presence of acids or bases (9,12). In order to assess the effect of seed particle acidity on SOA formation, α -pinene ozonolysis was carried out in the presence of both neutral and acidic ammonium sulfate seed as well as magnesium sulfate seed. The choice of these seeds allowed the study of the effect of seed type and pH on possible aerosol-phase reactions. The pH values of the bulk solutions from which the seeds were prepared from (at 55% relative humidity) are tabulated in Table 4 (9). During acid runs, sulfate fragmentation patterns in the mass spectra were analyzed to ascertain the acidity of the seed. Sulfate fragmentation patterns for pure and acidic ammonium sulfate were very similar since the most probable form of the anion in both systems is bisulfate. However, during acid MgSO_4 experiments, at least an order of magnitude increase in signals at fragments that are dominant for H_2SO_4 , namely m/z 81 (HSO_3^+) and m/z 98 (H_2SO_4^+), relative to the SO^+ fragment was observed.

As mentioned earlier, recent studies have shown evidence of polymerization and presence of high molecular weight species in SOA (9,11,12). Organic mass spectra obtained from the AMS are also suggestive of the presence of higher molecular weight fragments in SOA. Figure 10.10 indicates the relative contribution of higher molecular weight fragments to the total organic mass observed during α -pinene ozonolysis experiments in the presence of different seeds. The difference in contribution of larger fragments to the organic mass can be an indication of the presence of higher molecular

weight species in the SOA or presence of molecules that are more resistant to fragmentation. The difference between experiments with ammonium sulfate and acidic ammonium sulfate is statistically insignificant. In addition, the fragmentation patterns of SOA, analyzed with the time series of delta values, during these experiments are very similar. This can be explained since the pH difference between the ammonium sulfate and acidic ammonium sulfate solutions used is only ~ 2.2 , and thus the sensitivity of the two systems to acid-catalyzed reactions is not significantly different. The contribution of larger organic fragments to the organic mass increased, however, by 13% in the presence of acidic MgSO_4 seed as compared to pure MgSO_4 seed. This indicates that acid-catalyzed heterogeneous reactions that form high molecular weight species occur to a larger extent in the presence of acidic MgSO_4 seed, leading to a greater contribution of larger fragments to the total organic mass. Similar observations have been made during these experiments in terms of the percentage of increased organic yield of α -pinene in the presence of ozone and the same pairs of seed: presence of sulfuric acid with MgSO_4 seed led to an increased organic yield of 7-15%, while presence of sulfuric acid with ammonium sulfate seed led to an increased yield of $<5\%$ (9). Because of slower evaporation of the MgSO_4 (neutral or acidic) seed on the AMS vaporizer compared to ammonium sulfate, and to avoid build up of the salt on the vaporizer, the vaporizer temperature was increased to ~ 750 °C during experiments with MgSO_4 seed. Since organic species are expected to fragment to a greater extent at higher temperatures (32), it is possible to compare mass spectra of SOA only from experiments during which the AMS vaporizer is operated at the same temperature. For example, the degree, if any, to which slightly more acidic pure ammonium sulfate seed might have increased the degree

of polymerization compared to pure MgSO_4 seed cannot be inferred from Figure 10.10 because the AMS vaporizer was operated at a higher temperature with MgSO_4 seed and thus shifted the fragmentation of SOA towards smaller fragments.

Differences of fragmentation patterns are observed, as shown in Figure 10.11. For example, the contribution of $\Delta = -1$ and $\Delta = 3$ during acid MgSO_4 runs is lower while that of $\Delta=0$ is higher when comparing to the non-acid MgSO_4 runs (Figure 10.11a). These variations are consistent with suggested acid-catalyzed reaction mechanisms, e.g., acid-catalyzed gem-diol reactions as well as acid dehydration of monomers in α -pinene ozonolysis. Polymerization through gem-diol reaction involves the reaction of hydroxyl and carbonyl groups of monomers. Such reaction of α -pinene oxidation products that still contain one of the cyclic structures of α -pinene would result in a lower contribution of $\Delta = -1$ patterns to the oligomers. Acid dehydration in the aerosol phase would also lead to less contribution of organic acids/diacids to the total organic mass, and therefore less contribution of m/z 44 (CO_2^+ ion fragment) and $\Delta = 3$ to the total organic signal. Figure 10.11b shows the correlation of the reduction in $\Delta = 3$ fragments with decrease in CO_2^+ signal (m/z 44), which is attributed to thermal decomposition of oxygenated organic molecules, such as carboxylic acids or peroxides. This reduction is thus consistent with the acid dehydration mechanism. Furthermore, Tolocka *et al.* (10) outlined a mechanism of acid-catalyzed ring cleavage of primary ozonolysis products of α -pinene. The ring cleavage, which leads to smaller unsaturated oxidized molecules (such as ketones, aldehydes, or alcohols) with dominant $\Delta = 0$ patterns, may explain the increased contribution of $\Delta = 0$ patterns under acidic conditions (Figure 10.11a).

10.6.3. Photooxidation of *m*-xylene

The photooxidation of *m*-xylene was studied in the presence of pure and acidic ammonium sulfate seed, 45 ppb of NO, 15 ppb of NO₂, and 240 ppb of propene. Due to the nature of photooxidation experiments, i.e., simultaneous reactions in the two chambers with different seed aerosols, the AMS sampled alternatively from each chamber. In contrast to the morphology of SOA formed during cycloalkene ozonolysis but similar to biogenic SOA, SOA condensed on the seed during *m*-xylene photooxidation caused the sulfate seed signal to decrease, indicating poorer collection efficiency of the seed after SOA condensation, likely due to formation of solid phase SOA under the AMS vacuum conditions.

Figure 10.12 shows the evolution of the contribution of different ion series to the total organic signal during the experiment. Similar to pure ammonium sulfate and acidic ammonium sulfate experiments with α -pinene, there is little variation between the two seed types. Unlike ozonolysis of α -pinene, however, the contribution of $\Delta = 3$ increased by $\sim 16\%$ and $\sim 30\%$, during non-acid and acid experiments, respectively, over a similar time period after the start of reaction, as did the contribution of organic signal from m/z 44 (CO₂⁺ ion fragment), indicating a more prolonged oxidation process of the organics during the photooxidation study (Figure 10.12b).

Previous work on the composition of SOA formed under low-humidity photooxidation of *m*-xylene identified 3-methyl-2,5-furandione, *m*-toluic acid, and 2,5-furandione together with some nitrophenol compounds as the dominant species, contributing respectively to 61%, 9.2%, 5.2%, and 5.8% of the identified mass (33). The mass spectra obtained by the AMS exhibited increase in signals at m/z 54 and 68 that are

consistent with presence of 2,5-furandione and 3-methyl-2,5-furandione (Figure 10.13). Based on the contribution of m/z 68 to the total organic signal while sampling from the chamber and for pure 3-methyl-2,5-furandione during an off-line calibration procedure, the estimated mass of 3-methyl-2,5-furandione in *m*-xylene experiment was at most ~6 % of the total organic mass. It is not possible though to compare this estimate directly with that of Forstner *et al.* (33) because of the following reasons: (1) the humidity levels in the two sets of experiments are not the same; this is an important factor to consider since anhydrides tend to form carboxylic acids in the presence of water molecules (34); (2) percentage of the identified mass relative to total SOA mass has not been reported by Forstner *et al.* Also shown in Figure 10.13 are the time trends of fragments at m/z 30 and 46, two dominant fragments of nitrate. The increased signal intensity of these fragments after start of the reaction is consistent with the presence of nitro compounds in the SOA. The mass of 2,6-dimethyl-4-nitrophenol, identified in previous photooxidation studies of *m*-xylene, was estimated to be at most ~2% of the total organic mass based on the contribution of m/z 137 and 167 fragments to the total organic signal during an off-line calibration of pure 2,6-dimethyl-4-nitrophenol by the AMS. Although care has been taken to use fragments that do not have signal contributions from known inorganic compounds, the calculated contributions of 3-methyl-2,5-furandione and 2,6-dimethyl-4-nitrophenol to the total organic mass may be overestimated since some other organic species may also fragment at the masses used in these calculations.

10.7. Common Features in Different Systems

The patterns observed in the mass spectra of chamber-derived SOA for groups of precursors such as cycloalkenes and terpenes demonstrate that similar mixture of species

produce roughly similar mass spectra in the AMS. Organic mass spectra obtained from oxidation of α -pinene, *m*-xylene, and cyclopentene are compared in Figure 10.14 with those obtained in the ambient, sampling Ohio background pollution, measured airborne during Aug. 2004, Cleveland, OH pollution, obtained on the ground at the Cleveland International Airport during Aug. 2004, and brush-fire plumes, obtained in the vicinity of Monterey, CA during July 2003. All the ambient samples are dominated by signals at m/z 18 and 44 (similar to *m*-xylene and cyclopentene) and yet there is significant contribution from fragments at m/z 27, 29, 41, 43, and 55 in all cases. Furthermore, ambient mass spectra show a more dominant feature at m/z 57 compared to chamber-derived SOA, indicating greater presence of the alkyl groups in the ambient organic aerosols. The mass spectrum of the brush-fire plume also indicates signals at m/z 67 and 69, similar to that of α -pinene, which are common for unsaturated hydrocarbons, unsaturated alcohols, or unsaturated carbonyl groups.

Similarities between organic composition of the brush fire, Cleveland pollution, and background Ohio pollution plumes are apparent in the distribution of delta values obtained from the corresponding mass spectra as well (Figure 10.15). The dominant fragments in these mass spectra are those with $\Delta=2$ (alkyl groups and saturated carbonyls), $\Delta=0$ (unsaturated hydrocarbons, unsaturated alcohols, and unsaturated carbonyls), $\Delta=3$ (oxygenated organics and nitro compounds), and $\Delta=-1$. In addition, the organic mass spectra obtained from brush fire plumes show more contribution from fragments with negative delta values compared to the mass spectra of Cleveland and background Ohio pollution, indicating presence of more terpene derivative, aromatic, unsaturated, or cyclic structures. Similar dominance of fragments with delta values of

$\Delta=0, 2,$ and 3 has been observed in the organic mass spectra obtained during other ambient studies (17,35). The average delta values of different size fragments from ambient organic mass spectra are compared in Figure 10.16. Commonly, the larger fragments exhibit negative average delta values, indicating dominance of unsaturated, aromatic, or cyclic structures, while the smaller fragments have positive delta values, indicating dominance of more saturated and oxygenated structures.

In previous studies with the AMS, fragments at m/z 44 (CO_2^+ fragment of oxygenated organics) and m/z 57 (common fragment of alkyl groups) have been identified as indicators for oxygenated and hydrocarbon-like organic aerosols, respectively (14,19,36-38). Keeping in mind that the spectra obtained in chamber studies are all SOA spectra, for comparison purposes and as a reference, the relative contributions of these fragments to the total organic mass in several systems studied here are presented in Table 5.

10.8. Acknowledgement

This research was funded by the U.S. Environmental Protection Agency Science to Achieve Results (STAR) Program grant number RD-83107501-0, managed by EPA's Office of Research and Development (ORD), National Center for Environmental Research (NCER), U.S. Department of Energy Biological and Environmental Research Program DE-FG03-01ER63099, and by the National Science Foundation grant ATM-0340832. The authors thank J.D. Allan (UMIST) for fundamental AMS data analysis software, M.R. Canagaratna and T. Onasch (Aerodyne Research, Inc.) for developing the software for ion series analysis of AMS data, and F. Brechtel (Caltech and Brechtel Manufacturing Inc.) for helpful discussions.

10.9. References

- (1) Pandis, S. N.; Paulson, S. E.; Seinfeld, J. H.; Flagan, R. C. Aerosol formation in the photooxidation of isoprene and b-pinene. *Atmospheric Environment*, **1991**, *25*(5-6), 997-1008.
- (2) Hoffmann, T.; Odum, J. R.; Bowman, F. M.; Collins, D.; Klockow, D.; Flagan, R. C.; Seinfeld, J. H. Formation of organic aerosols from the oxidation of biogenic hydrocarbons. *J. of Atmospheric Chemistry*, **1997**, *26*(2), 189-222.
- (3) Odum, J. R.; Jungkamp, T. P. W.; Griffin, R. J.; Flagan, R. C.; Seinfeld, J. H. The atmospheric aerosol-forming potential of whole gasoline vapor. *Science*, **1997**, *276*(5309), 96-99.
- (4) Odum, J. R.; Jungkamp, T. P. W.; Griffin, R. J.; Forstner, H. J. L.; Flagan, R. C.; Seinfeld, J. H. Aromatics, reformulated gasoline, and atmospheric organic aerosol formation. *Environ. Sci. Technol.*, **1997**, *31*(7), 1890-1897.
- (5) Griffin, R. J.; Cocker, D. R.; Flagan, R. C.; Seinfeld, J. H. Organic aerosol formation from the oxidation of biogenic hydrocarbons. *J. Geophys. Res.*, **1999**, *104*(D3), 3555-3567.
- (6) Keywood, M. D.; Varutbangkul, V.; Bahreini, R.; Flagan, R. C.; Seinfeld, J. H. Secondary organic aerosol formation from the ozonolysis of cycloalkenes and related compounds. *Environ. Sci. Technol.*, **2004**, *38*, 4157-4164.
- (7) Kalberer, M.; Paulsen, D.; Sax, M.; Steinbacher, M.; Dommen, J.; Prevot, A. S. H.; Fiesseha, R.; Weingartner, E.; Frankevich, V.; Zenobi, R.; Baltensperger, U. Identification of polymers as major components of atmospheric organic aerosols. *Science*, **2004**, *303*, 1659-1662.

- (8) Limbeck, A.; Kulmala, M.; Puxbaum, H. Secondary organic aerosol formation in the atmosphere via heterogeneous reaction of gaseous isoprene on acidic particles. *Geophys. Res. Letter*, **2003**, *30(19)*, 1996, doi:1910.1029/2003GL017738.
- (9) Gao, S.; Ng, N. L.; Keywood, M.; Varutbangkul, V.; Bahreini, R.; Nenes, A.; He, J.; Yoo, K. Y.; Flagan, R. C.; Seinfeld, J. H. Particle phase acidity and oligomer formation in secondary organic aerosol. *Environ. Sci. Technol.*, **2004**, doi: 10.1021/es049125k.
- (10) Tolocka, M. P.; Jang, M.; Ginter, J. M.; Cox, F. J.; Kamens, R. M.; Johnston, M. V. Formation of oligomers in secondary organic aerosol. *Environ. Sci. Technol.*, **2004**, *38*, 1428-1434.
- (11) Gao, S.; Keywood, M.; Ng, N. L.; Surratt, J.; Varutbangkul, V.; Bahreini, R.; Flagan, R. C.; Seinfeld, J. H. Low-molecular-weight and oligomeric components in secondary organic aerosol from the ozonolysis of cycloalkenes and α -pinene. *J. Phys Chem.*, **2004**, 10.1021/jp047466e.
- (12) Jang, M.; Czoschke, N. M.; Lee, S.; Kamens, R. M. Heterogeneous atmospheric aerosol production by acid-catalyzed particle-phase reactions. *Science*, **2002**, *298*, 814-817.
- (13) Jayne, J. T.; Leard, D. C.; Zhang, X.; Davidovits, P.; Smith, K. A.; Kolb, C. E.; Worsnop, D. W. Development of an Aerosol Mass Spectrometer for size and composition analysis of submicron particles. *Aerosol Science and Technology*, **2000**, *33*, 49-70.
- (14) Jimenez, J. L.; Jayne, J. T.; Shi, Q.; Kolb, C. E.; Worsnop, D. R.; Yourshaw, I.; Seinfeld, J. H.; Flagan, R. C.; Zhang, X.; Smith, K. A.; Morris, J.; Davidovits, P.

- Ambient aerosol sampling with an Aerosol Mass Spectrometer. *J. Geophys. Res.*, **2003**, *108(D7)*, 8425, doi:8410.1029/2001JD001213.
- (15) Bahreini, R.; Jimenez, J. L.; Wang, J.; Flagan, R. C.; Seinfeld, J. H.; Jayne, J. T.; Worsnop, D. R. Aircraft-based aerosol size and composition measurements during ACE-Asia using an Aerodyne aerosol mass spectrometer. *J. Geophys. Res.*, **2003**, *108(D23)*, 8645, doi:8610.1029/2002JD003226.
- (16) Allan, J. D.; Bower, K. N.; Coe, H.; Boudries, H.; Jayne, J. T.; Canagaratna, M. R.; Millet, D. B.; Goldstein, A. H.; Quinn, P. K.; Weber, R. J.; Worsnop, D. R. Submicron aerosol composition at Trinidad Head, California, during ITCT 2K2: Its relationship with gas phase volatile organic carbon and assessment of instrument performance. *J. Geophys. Res.*, **2004**, *109(23)*, D23S24, doi:10.1029/2003JD004208.
- (17) Drewnick, F.; Schwab, J. J.; Jayne, J. T.; Canagaratna, M.; Worsnop, D. R.; Demerjian, K. L. Measurements of ambient aerosol composition during PMTACS-NY 2001 using an aerosol mass spectrometer. Part I: Mass Concentrations. *Aerosol Science and Technology*, **2004**, *38(S1)*, 92-103.
- (18) Drewnick, F.; Schwab, J. J.; Jayne, J. T.; Canagaratna, M.; Worsnop, D. R.; Demerjian, K. L. Measurements of ambient aerosol composition during PMTACS-NY 2001 using an aerosol mass spectrometer. Part II: Chemically speciated mass distributions. *Aerosol Science and Technology*, **2004**, *38(S1)*, 104-117.
- (19) Zhang, Q.; Stanier, C. O.; Canagaratna, M.; Jayne, J. T.; Worsnop, D. R.; Pandis, S. N.; Jimenez, J. L. Insights into the chemistry of nucleation bursts and new particle growth events in Pittsburgh based on aerosol mass spectrometry. *Environ. Sci. Technol.*, **2004**, *38*, 4797-4809.

- (20) O'Dowd, C. D.; Jimenez, J. L.; Bahreini, R.; Flagan, R. C.; Seinfeld, J. H.; Hameri, K.; Pirjola, L.; Kulmala, M.; Jennings, S. G.; Hoffmann, T. Marine aerosol formation from biogenic iodine emissions. *Nature*, **2002**, *417*, 632-636.
- (21) Jimenez, J. L.; Bahreini, R.; Cocker, D. R.; Zhuang, H.; Varutbangkul, V.; Flagan, R. C.; Seinfeld, J. H.; O'Dowd, C. D.; Hoffmann, T. New Particle Formation from Photooxidation of Diiodomethane (CH_2I_2). *J. Geophys. Res.*, **2003**, *108(D10)*, 4318, doi:4310.1029/2002JD002452.
- (22) Alfarra, M. R.; Paulsen, D.; Gysel, M.; Garforth, A. A.; Dommen, J.; Prevot, A. S. H.; Worsnop, D. R.; Baltensperger, U.; Coe, H. A mass spectrometric study of secondary organic aerosols formed from the photooxidation of anthropogenic and biogenic precursors in a reaction chamber. *Submitted to Environ. Sci. Technol.*, **Oct. 2004**.
- (23) Cocker, D. R.; Flagan, R. C.; Seinfeld, J. H. State-of-the-art chamber facility for studying atmospheric aerosol Chemistry. *Environ. Sci. Technol.*, **2001**, *35*, 2594-2601.
- (24) Allan, J. D.; Jimenez, J. L.; Coe, H.; Bower, K. N.; Williams, P. I.; Worsnop, D. R. Quantitative sampling using an Aerodyne Aerosol Mass Spectrometer. Part 1: Techniques of data interpretation and error analysis. *J. Geophys. Res.*, **2003**, *108(D3)*, 4090, doi:4010.1029/2002JD002358.
- (25) Allan, J. D.; Delia, A. E.; Coe, H.; Bower, K. N.; Alfarra, M. R.; Jimenez, J. L.; Middlebrook, A. M.; Drewnick, F.; Onasch, T. B.; Canagaratna, M. R.; Jayne, J. T.; Worsnop, D. R. A generalized method for the extraction of chemically resolved mass spectra from aerodyne aerosol mass spectrometer data. *J. Aerosol Science*, **2004**, *35(7)*, 909-922.

- (26) Wang, S. C.; Flagan, R. C. Scanning electrical mobility spectrometer. *J. Aerosol Science*, **1989**, *20(8)*, 1485-1488.
- (27) Keywood, M. D. K.; Kroll, J. H.; Varutbangkul, V.; Bahreini, R.; Flagan, R. C.; Seinfeld, J. H. Secondary Organic Aerosol Formation from Cyclohexene Ozonolysis: Effect of OH Scavenger and the Role of Radical Chemistry. *Environ. Sci. Technol.*, **2004**, *38(12)*, 3343-3350.
- (28) Docherty, K. S.; Ziemann, P. J. Effects of stabilized Criegee intermediate and OH radical scavengers on aerosol formation from reactions of beta-pinene with O₃. *Aerosol Science and Technology*, **2003**, *37(11)*, 877-891.
- (29) Jimenez, J. L.; Bahreini, R.; Cocker, D. R.; Zhuang, H.; Varutbangkul, V.; Flagan, R. C.; Seinfeld, J. H.; O'Dowd, C. D.; Hoffmann, T. New particle formation from photooxidation of diiodomethane (CH₂I₂). *J. Geophys. Res.*, **2003**, *108(D23)*, 4733, doi:4710.1029/2003JD004249.
- (30) DeCarlo, P.; Slowik, J. G.; Worsnop, D. R.; Davidovits, P.; Jimenez, J. L. Particle morphology and density characterization by combined mobility and aerodynamic measurements. Part 1: Theory. *Aerosol Science and Technology*, **2004**, *38(DOI: 10.1080/027868290903907)*, 1185–1205.
- (31) McLafferty, F. W.; Turecek, F. In *Interpretation of Mass Spectra*; University Science Books: Sausalito, CA, 1993.
- (32) Alfarra, R.M., Insights Into Atmospheric Organic Aerosols Using An Aerosol Mass Spectrometer, Ph.D. Thesis, University of Manchester, **2004**.

- (33) Forstner, H. J. L.; Flagan, R. C.; Seinfeld, J. H. Secondary organic aerosol from the photooxidation of aromatic hydrocarbons: molecular composition. *Environ. Sci. Technol.*, **1997**, *31*, 1345-1358.
- (34) Koehler, C. A.; Fillo, J. D.; Ries, K. A.; Sanchez, J. T.; Haan, D. O. D. Formation of secondary organic aerosol by reactive condensation of furandiones, aldehydes, and water vapor onto inorganic aerosol seed particles. *Environ. Sci. Technol.*, **2004**, *38*, 5064-5072.
- (35) Schneider, J.; Borrmann, S.; Wollny, A. G.; Blasner, M.; Mihalpoulos, N.; Oikonomou, K.; Sciare, J.; Teller, A.; Levin, Z.; Worsnop, D. R. Online mass spectrometric aerosol measurements during the MINOS campaign (Crete, August 2001). *Atmos. Chem. Phys.*, **2004**, *4*, 65-80.
- (36) Zhang, Q.; Alfarra, M. R.; Worsnop, D. R.; Allan, J. D.; Coe, H.; Canagaratna, M. R.; Jimenez, J. L. Deconvolution and quantification of primary and oxygenated organic aerosols based on aerosol mass spectrometry. Part I: Development and validation of the method. *Submitted to Environ. Sci. Technol.*, **Sep. 2004**.
- (37) Canagaratna, M.; Jayne, J. T.; Ghertner, D. A.; Herndon, S.; Shi, Q.; Jimenez, J. L.; Silva, P. J.; Williams, P.; Lanni, T.; Drewnick, F.; Demerjian, K. L.; Kolb, C. E. Chase Studies of Particulate Emissions from in-use New York City Vehicles. *Aerosol Science and Technology*, **2004**, *38*, 555-573.
- (38) Alfarra, M. R.; Coe, H.; Allan, J. D.; Bower, K. N.; Boudries, H.; Canagaratna, M. R.; Jimenez, J. L.; Jayne, J. T.; Garforth, A. A.; Li, S.; Worsnop, D. R. Characterization of urban and rural organic particulate in the Lower Fraser Valley using

two Aerodyne Aerosol Mass Spectrometers. *Atmospheric Environment*, **2004**, 38, 5745-5758.

Table 10.1. Summary of conducted experiments

Date	Parent Hydrocarbon	Initial Conc., ppb	Seed Aerosol	RH %
10/02/03	Cyclopentene, CP	173	(NH ₄) ₂ SO ₄	<10
05/31/04	CP	192	None	<10
10/8/03	1-methyl-cyclopentene, 1MCP	171	(NH ₄) ₂ SO ₄	<10
02/10/03	Cyclohexene, CHX	173	(NH ₄) ₂ SO ₄	<10
02/19/03	CHX	234	(NH ₄) ₂ SO ₄	<10
09/30/03	CHX	185	(NH ₄) ₂ SO ₄	<10
05/28/04	CHX	152	None	<10
02/04/03	Cycloheptene, CHP	212	(NH ₄) ₂ SO ₄	<10
02/19/03	CHP	282	(NH ₄) ₂ SO ₄	<10
03/24/03	CHP	184	(NH ₄) ₂ SO ₄	<10
09/30/03	CHP	186	(NH ₄) ₂ SO ₄	<10
05/28/04	CHP	170	None	<10
04/11/03	Cyclooctene, COCT	195	(NH ₄) ₂ SO ₄	<10
10/02/03	COCT		(NH ₄) ₂ SO ₄	<10
05/31/04	COCT	177	None	<10
01/27/03	1-methyl-cyclohexene, 1MCX	213	(NH ₄) ₂ SO ₄	<10
01/29/03	1MCX	205	(NH ₄) ₂ SO ₄	<10
02/10/03	1MCX	148	(NH ₄) ₂ SO ₄	<10
03/03/03	1MCX	257	(NH ₄) ₂ SO ₄	<10
10/06/06	1MCX	202	(NH ₄) ₂ SO ₄	<10
06/07/04	1MCX	159	None	<10
10/06/03	3-methyl-cyclohexene, 3MCX	183	(NH ₄) ₂ SO ₄	<10
06/07/04	3MCX	178	None	<10
10/08/03	1-methyl-cycloheptene, 1MCHP	170	(NH ₄) ₂ SO ₄	<10
06/02/04	1MCHP	169	None	<10
02/04/03	Methylene cyclohexane, MCHX	218	(NH ₄) ₂ SO ₄	<10
10/04/03	MCHX	181	(NH ₄) ₂ SO ₄	<10
06/02/04	MCHX	188	None	<10
05/18/04	<i>m</i> -xylene	143	(NH ₄) ₂ SO ₄	55
05/18/04	<i>m</i> -xylene	137	(NH ₄) ₂ SO ₄ +H ₂ SO ₄ ^a	55
03/24/03	α -pinene	186	(NH ₄) ₂ SO ₄	<10

Date	Parent Hydrocarbon	Initial Conc., ppb	Seed Aerosol	RH %
10/31/03	α -pinene	111	(NH ₄) ₂ SO ₄	55
10/31/03	α -pinene	113	(NH ₄) ₂ SO ₄ +H ₂ SO ₄ ^b	55
11/03/03	α -pinene	71	(NH ₄) ₂ SO ₄	55
11/03/03	α -pinene	72	(NH ₄) ₂ SO ₄ +H ₂ SO ₄ ^b	55
11/25/03	α -pinene	48	MgSO ₄	55
11/25/03	α -pinene	47	MgSO ₄ +H ₂ SO ₄ ^b	55
11/27/03	α -pinene	96	MgSO ₄	55
11/27/03	α -pinene	88	MgSO ₄ +H ₂ SO ₄ ^b	55
11/29/03	α -pinene	52	MgSO ₄	55
11/29/03	α -pinene	51	MgSO ₄ +H ₂ SO ₄ ^b	55
03/15/03	β -pinene	196	None	<10
03/31/03	Terpinolene	97	(NH ₄) ₂ SO ₄	<10
04/11/03	Terpinolene	188	(NH ₄) ₂ SO ₄	<10
06/04/04	Terpinolene	200	None	<10
03/31/03	α -Terpinene	58	None	<10
04/04/03	Δ^3 -carene	90	(NH ₄) ₂ SO ₄	<10
04/02/03	Myrcene	83	(NH ₄) ₂ SO ₄	<10
04/04/03	Allylanisole	120	(NH ₄) ₂ SO ₄	<10
04/02/03	Linalool	72	(NH ₄) ₂ SO ₄	<10
03/28/03	β -caryophyllene	89	None	<10
03/28/03	α -humulene	103	None	<10

^aAcidic seed made from 0.03 M salt+0.1 M H₂SO₄ solution

^bAcidic seed made from 0.03 M salt+0.05 M H₂SO₄ solution

Table 10.2. Estimated effective density of SOA during cycloalkene ozonolysis experiments in the presence or absence of seed aerosol. The corresponding standard deviations of the average when multiple experiments were considered are indicated in parentheses. (See Figure 10.1 for list of compounds)

ρ_{SOA} (g/cm ³)	CP	CHX	CHP	COCT	1MCP	1MCX	3MCX	MCHX	1MCHP
Seeded	1.15	1.13 (0.04)	1.14 (0.05)	1.14 (<0.01)	1.07	1.06 (0.08)	1.06	1.08 (0.06)	1.11
Nucleation	1.42	1.45	1.4	1.38	N/A	1.3	1.43	N/A	1.35

Table 10.3. Estimated effective density of SOA during biogenic ozonolysis experiments. The corresponding standard deviations of the average when multiple experiments were considered are indicated in parentheses. These densities are lower limits of the true material densities, as shape effects for these experiments tend to reduce the measured effective densities. All estimates are based on seeded experiments except for β -pinene, β -caryophyllene, and α -humulene (See Table 1).

Parent HC	ρ_{SOA} (g/cm ³)	Parent HC	ρ_{SOA} (g/cm ³)
Terpinolene ^a	1.29 (0.03)	4-allylanisole	1.04
α -pinene ^b	1.19	Linalool	0.64
β -pinene	1.20	β -caryophyllene	1.3
Δ^3 -carene	1.19	α -humulene	1.25
Myrcene	1.17		

^a Seeded experiments; ^b Experiment on 03/24/03

Table 10.4. Estimated pH values of seed particles and their relative bulk concentrations

	(NH ₄) ₂ SO ₄ (0.03 M)	(NH ₄) ₂ SO ₄ +H ₂ SO ₄ (0.03 M+ 0.05 M)	MgSO ₄ (0.03 M)	MgSO ₄ +H ₂ SO ₄ (0.03 M+ 0.05 M)
pH (RH=55%)	4.6	2.4	6.5	-0.3

Table 10.5. Relative contribution of different fragments to the total organic signal (See Table 1 for list of compounds and experiments)

Hydrocarbon	<i>m/z</i> 44	<i>m/z</i> 57	Hydrocarbon	<i>m/z</i> 44	<i>m/z</i> 57
CHX ^a	0.061	0.018	β -pinene	0.055	0.006
1MCX ^a	0.043	0.019	α -terpinene	0.058	0.008
CHP ^a	0.059	0.020	Terpinolene ^d	0.080	0.008
MCHX ^a	0.067	0.021	myrcene	0.063	0.011
COCT ^a	0.039	0.017	linalool	0.056	0.011
<i>m</i> -xylene ^b	0.149	0.004	α -humulene	0.037	0.012
α -pinene ^c	0.042	0.006	β -caryophyllene	0.042	0.008

^a Nucleation experiment; ^b Seeded experiment with ammonium sulfate; ^c Experiment on 3/24/03;
^d Seeded experiment

Figure 10.1. Chemical structures of the SOA precursor compounds studied

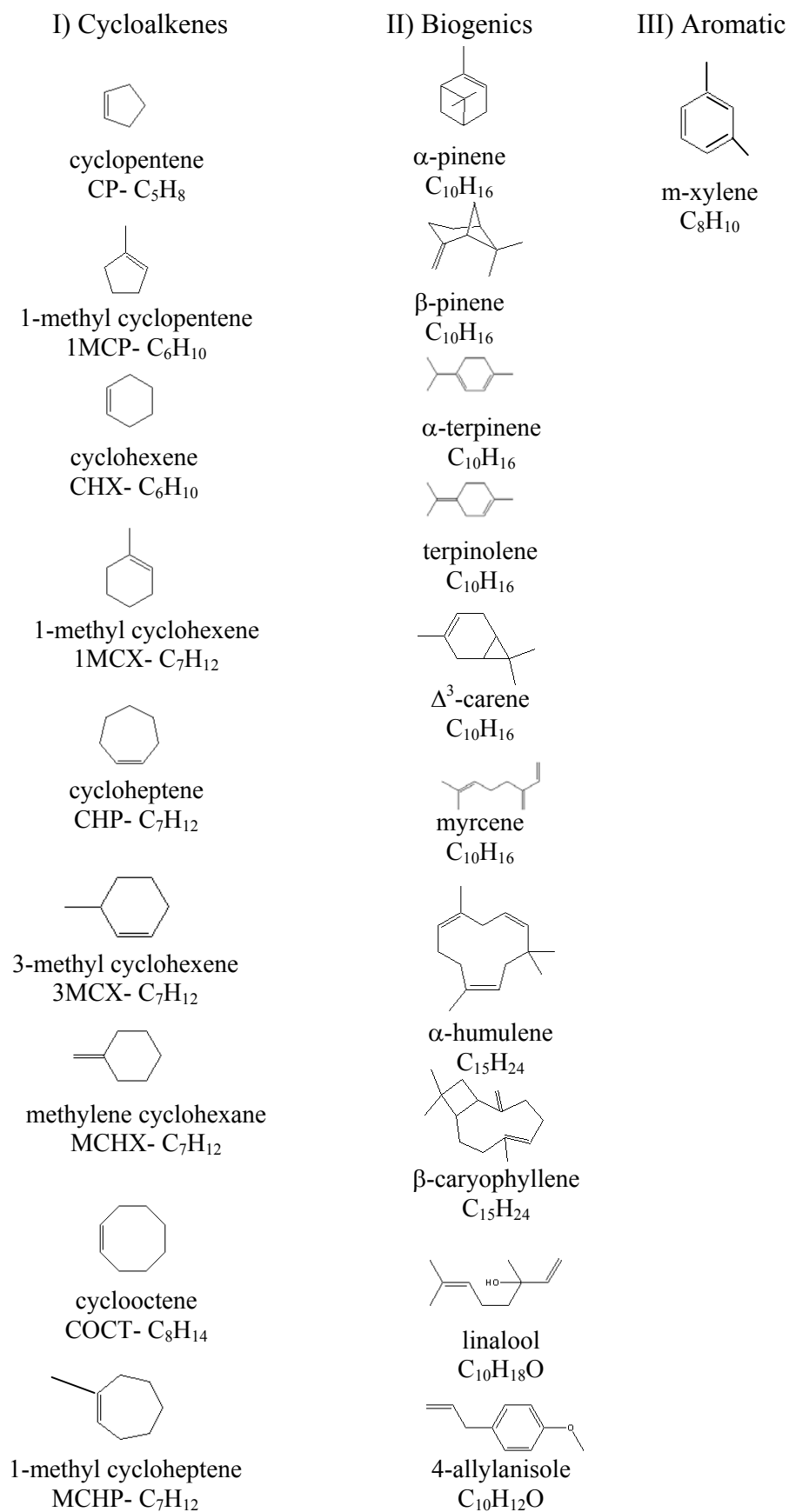
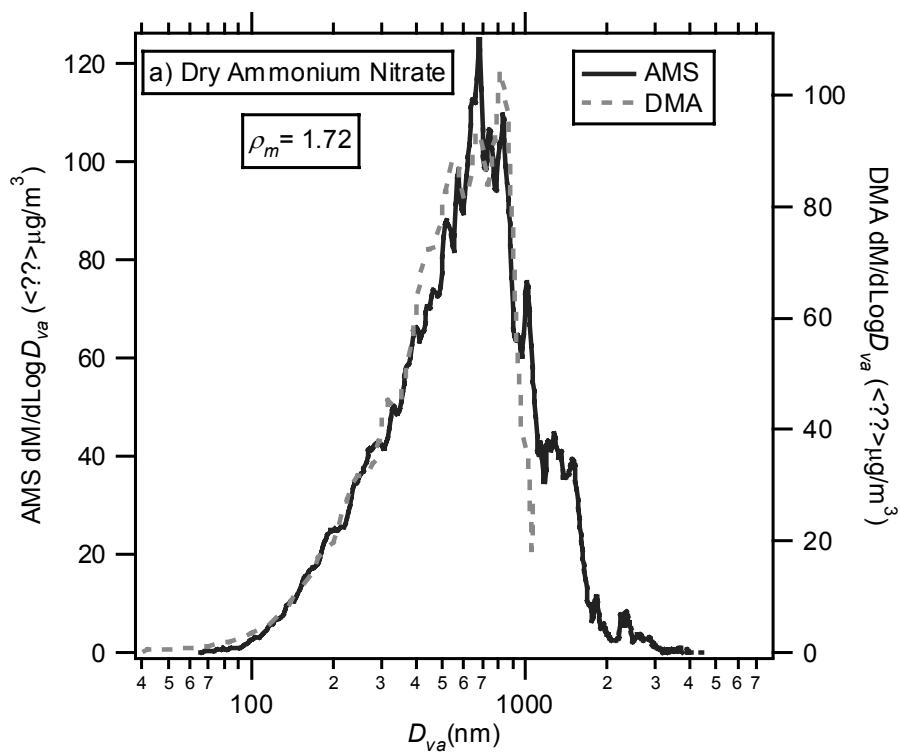


Figure 10.2. Comparison of AMS and DMA mass distributions as a means to deduce aerosol effective density: AMS and DMA Mass distributions of (a) dry ammonium nitrate ($\rho_{\text{NH}_4\text{NO}_3}=1.72$); (b) dry ammonium sulfate ($\rho_{(\text{NH}_4)_2\text{SO}_4}=1.77$); (c) SOA formed during cyclooctene ozonolysis ($\rho_m=1.18$)



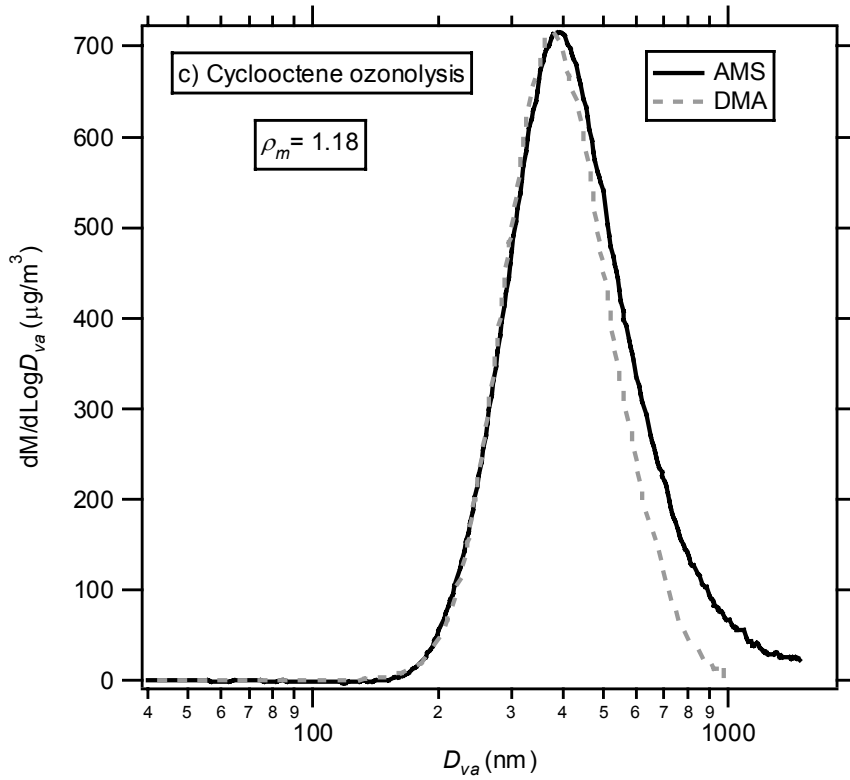
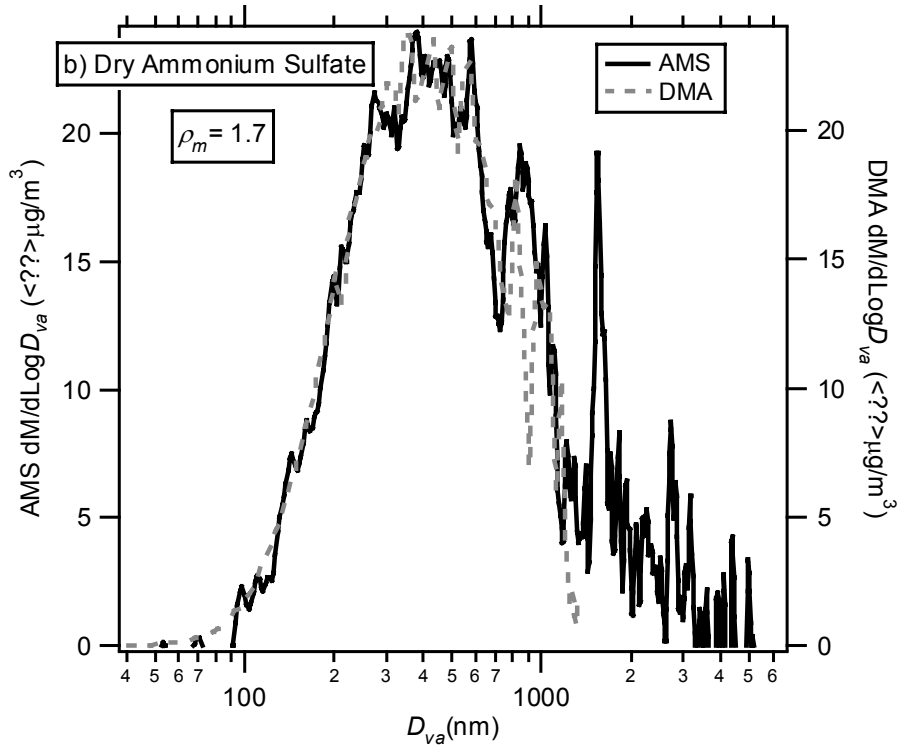
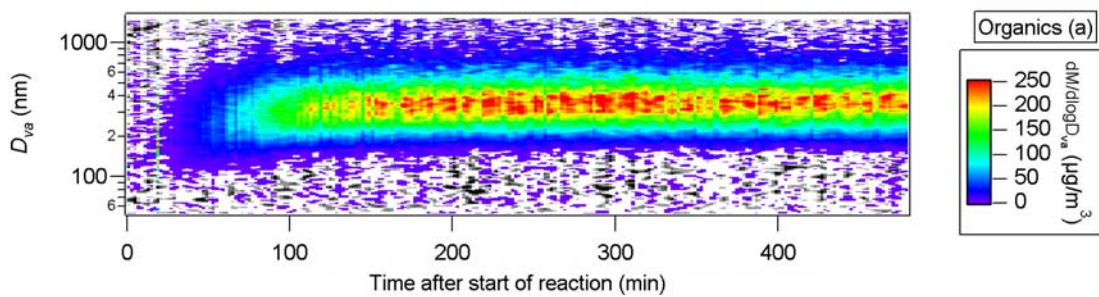
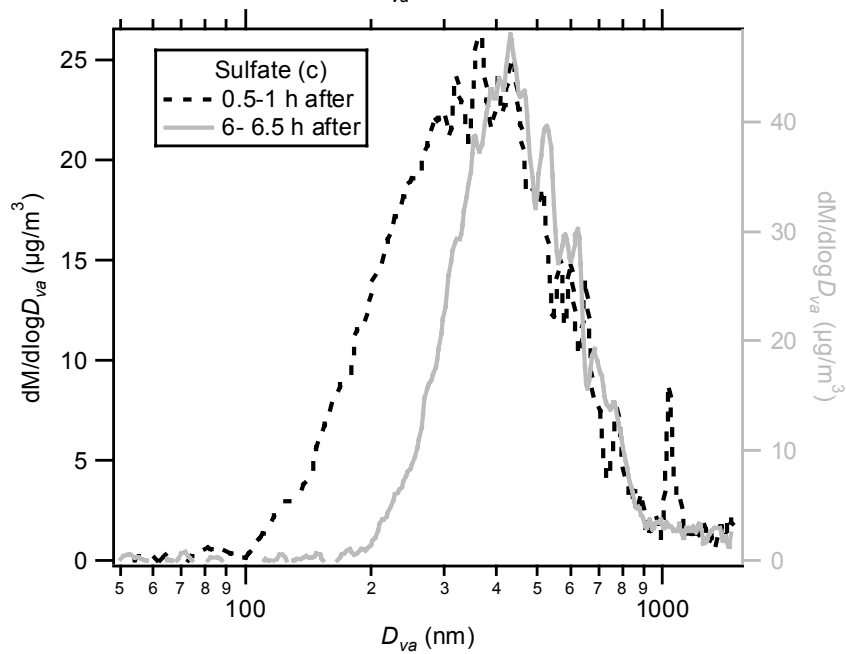
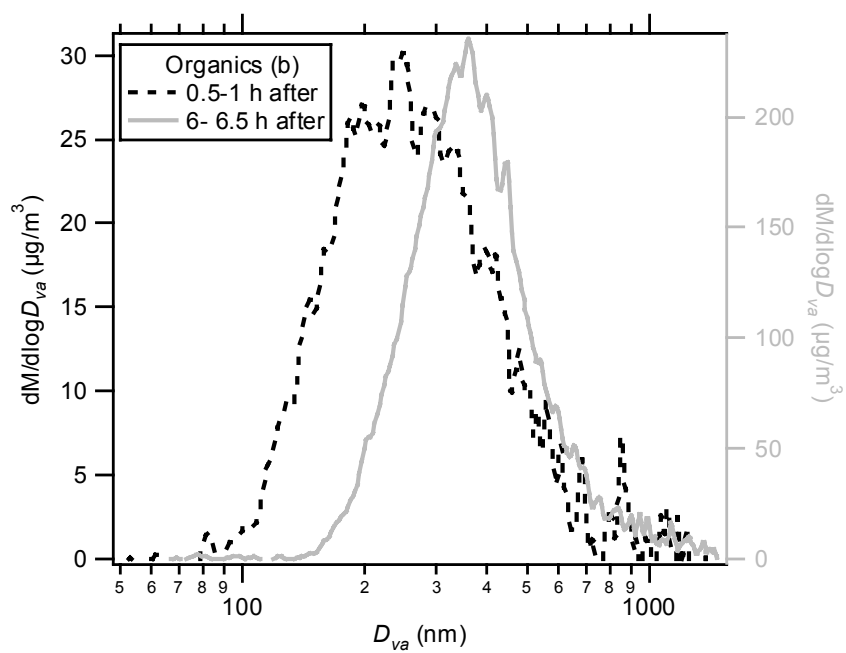


Figure 10.3. Evolution of mass distributions of organics and sulfate (a-c) and the mass spectra (d-e) during cyclohexene ozonolysis. SOA formation led to growth of aerosols with narrower mass distributions and increased organic signal intensities in the mass spectra.





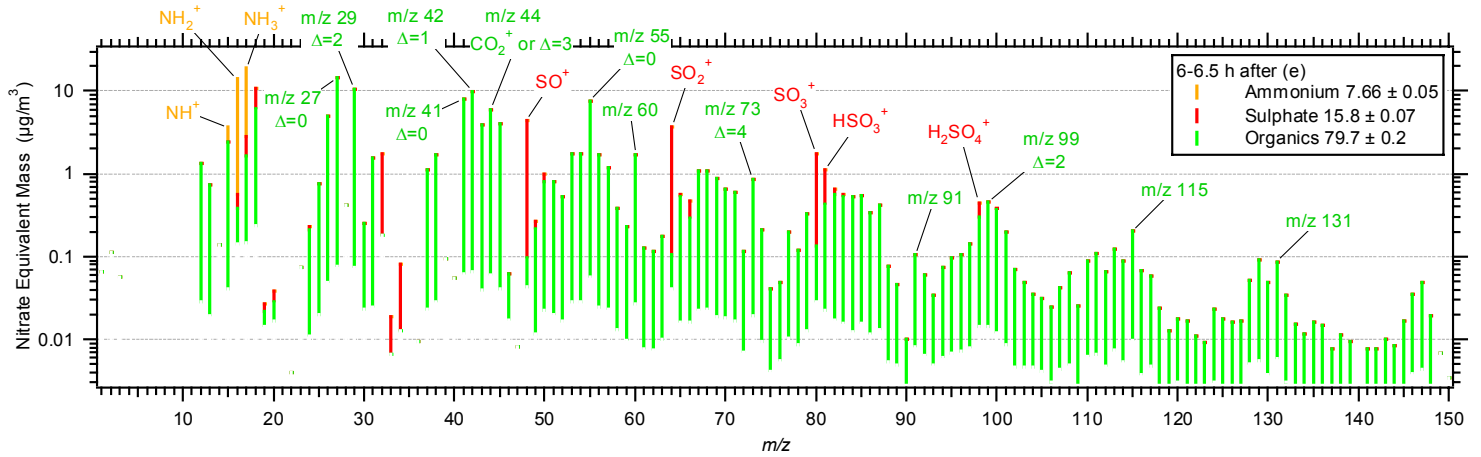
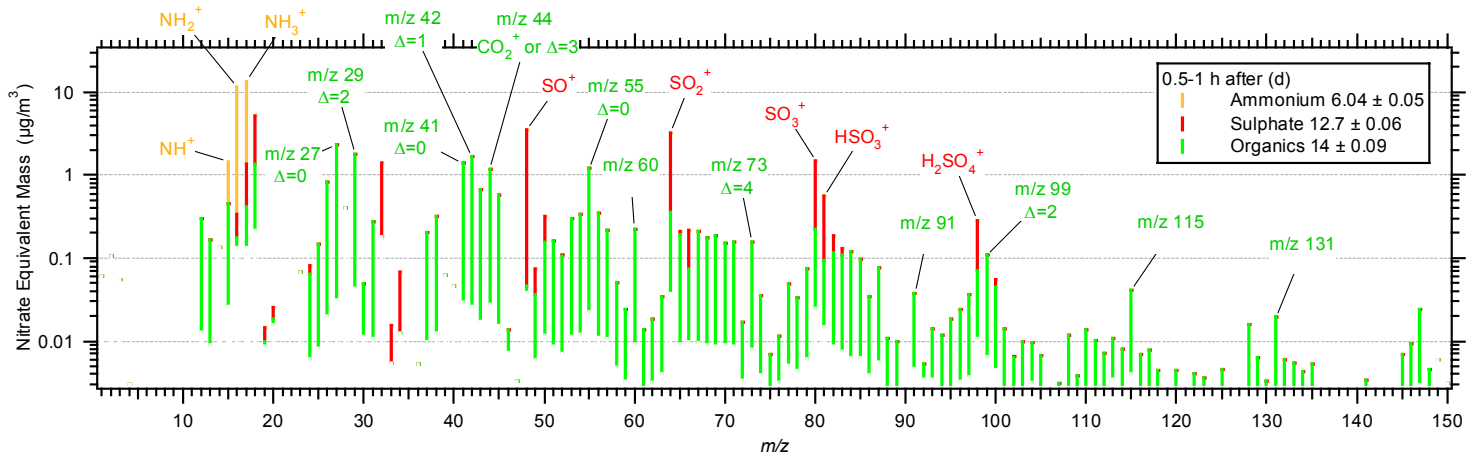


Figure 10.4. Time trends of sulfate and organic mass concentrations during cyclopentene ozonolysis. Sulfate signal increased after SOA formation, indicating improved collection efficiency of organic-coated seed particles.

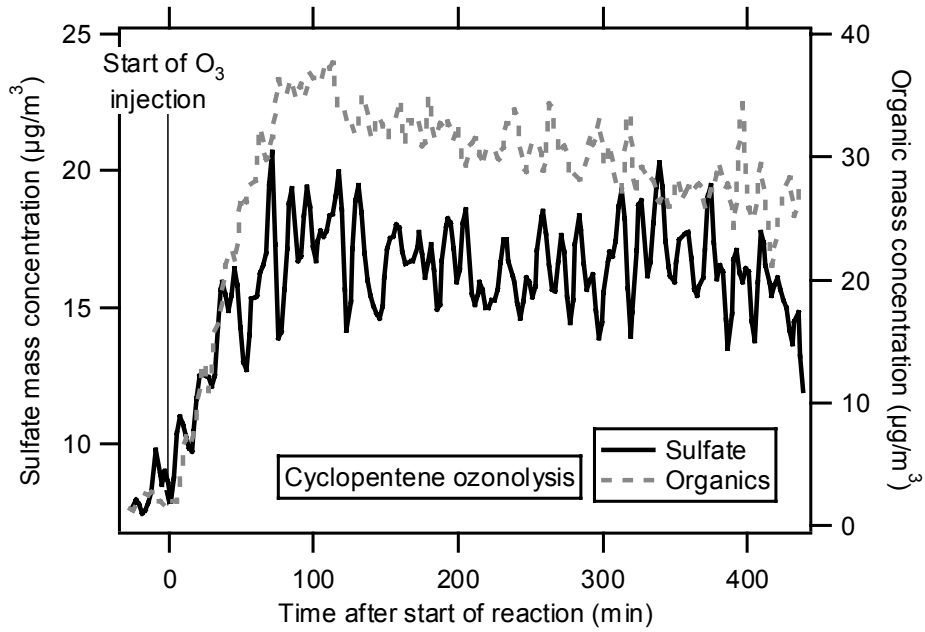


Figure 10.5. Fraction of the organic signal at $\Delta=4$ (common Δ group for $C_nH_{2n-1}O_2^+$ fragment of acids) and m/z 44 (CO_2^+ fragment of oxygenated organics) in total SOA mass during initial stages of cycloheptene oxidation. Increased contribution of carboxylic acid fragments to total mass during initial stages of nucleation experiments may explain higher SOA density observed in these experiments.

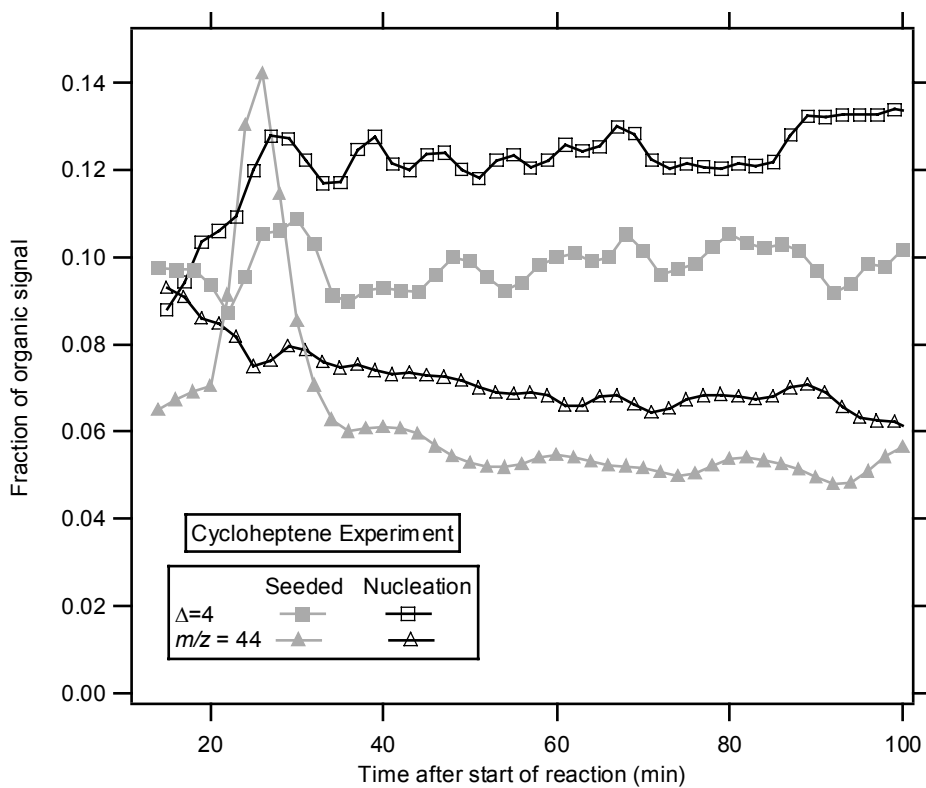
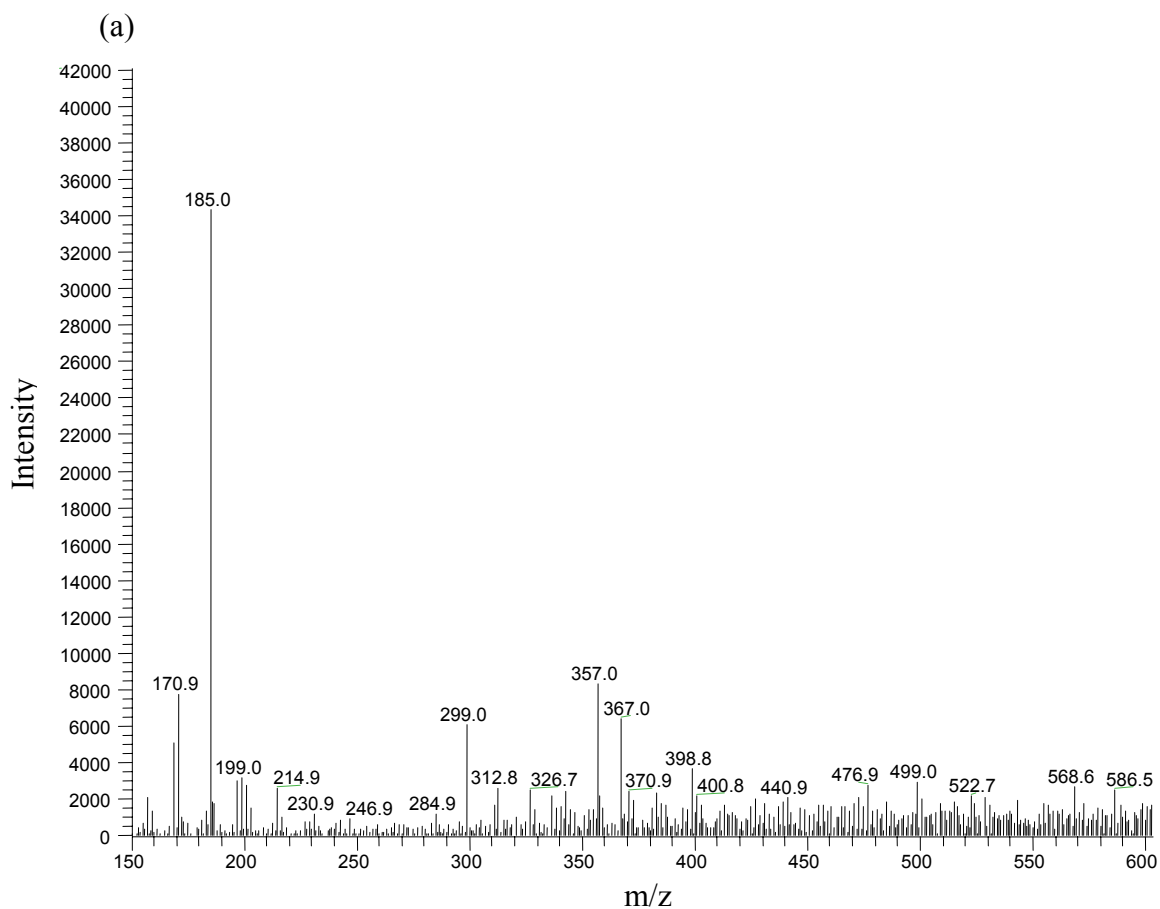


Figure 10.6. Ion trap mass spectra (negative-ion mode) of SOA from α -pinene (100 ppb) ozonolysis; (a) in the presence of MgSO_4 seed particles; (b) in the absence of any seed particles. The mass spectrum of SOA formed during nucleation exhibits higher signal intensity for acids (m/z 171, 185, 199) and oligomers (m/z 299, 357, and 399) than the seeded experiment.



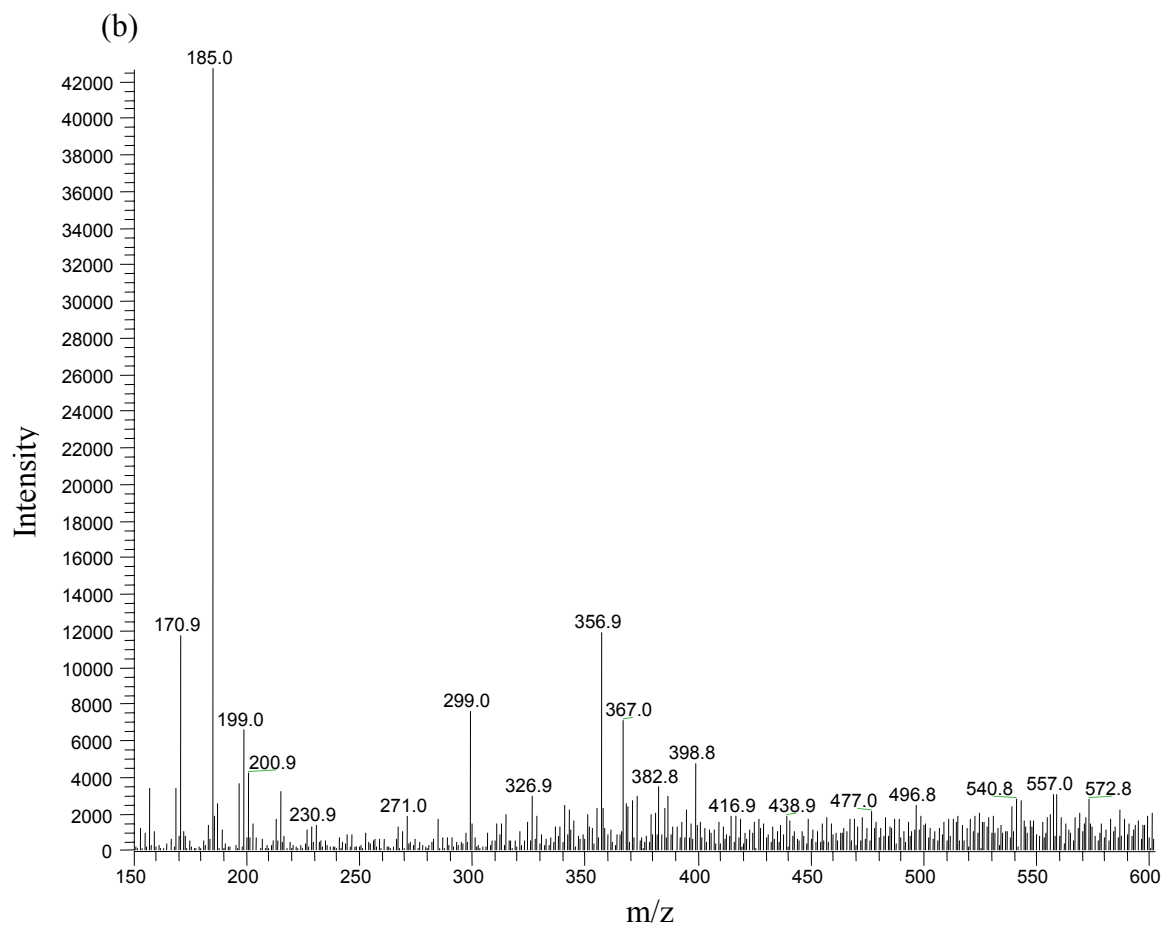


Figure 10.7. Relationship between SOA effective density with relative contribution of m/z 44 signal to total organic signal for different classes of parent hydrocarbons. Increased SOA effective density is observed with increased contribution of m/z 44 (CO_2^+ fragment of oxygenated organics) to total organic signal.

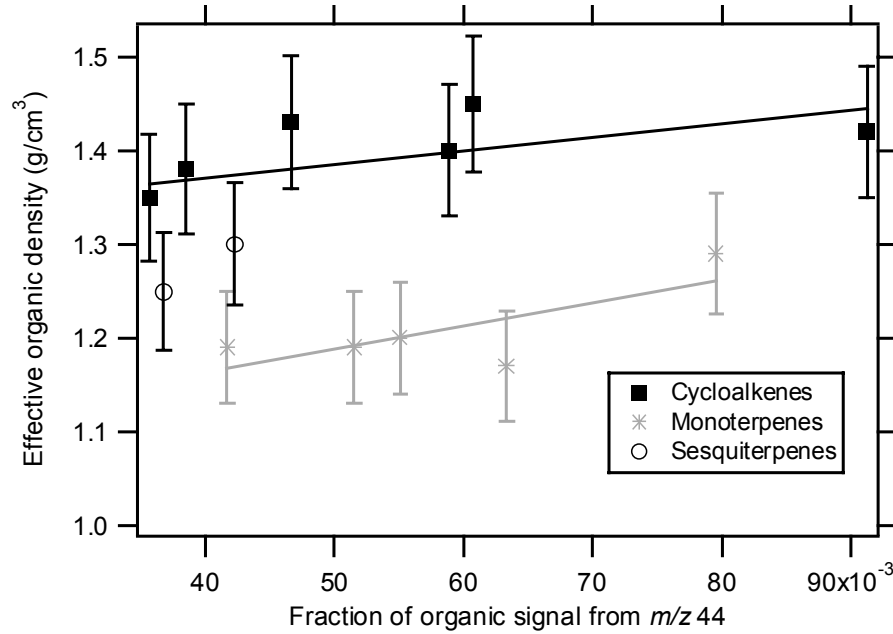


Figure 10.8. Time trends of sulfate and organic mass concentrations in ozonolysis of linalool. Decrease in sulfate signal after SOA formation indicates poorer collection efficiency of particles, and may suggest formation of solid SOA.

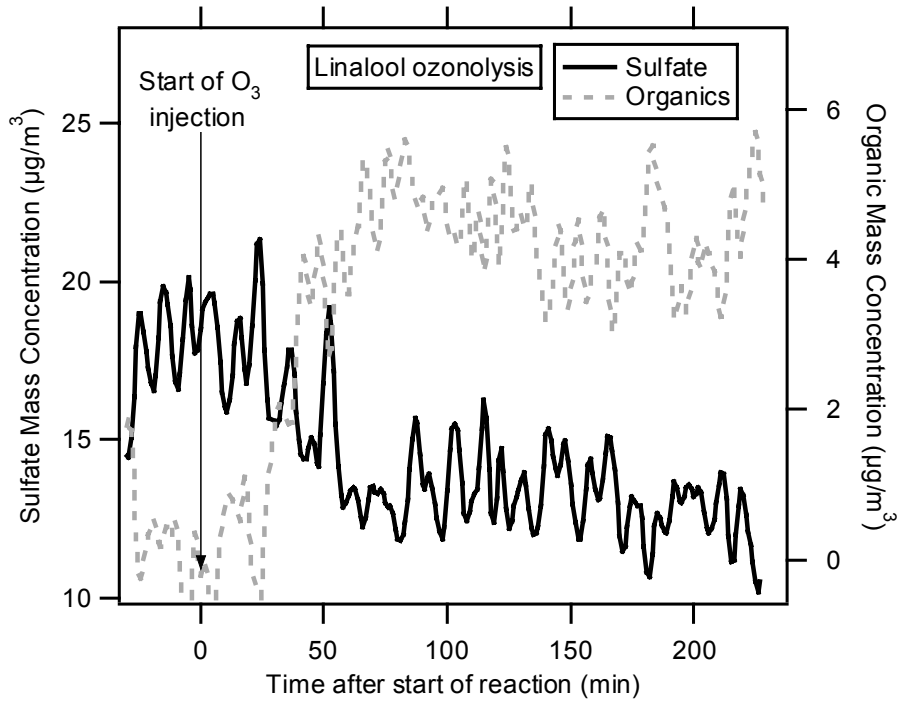


Figure 10.9. Average delta values of different size fragments for anthropogenic and biogenic SOA. In contrast to anthropogenic SOA, larger fragments of biogenic SOA have dominantly negative Δ values, indicating presence of terpene derivative structures and unsaturated or cyclic oxygenated compounds.

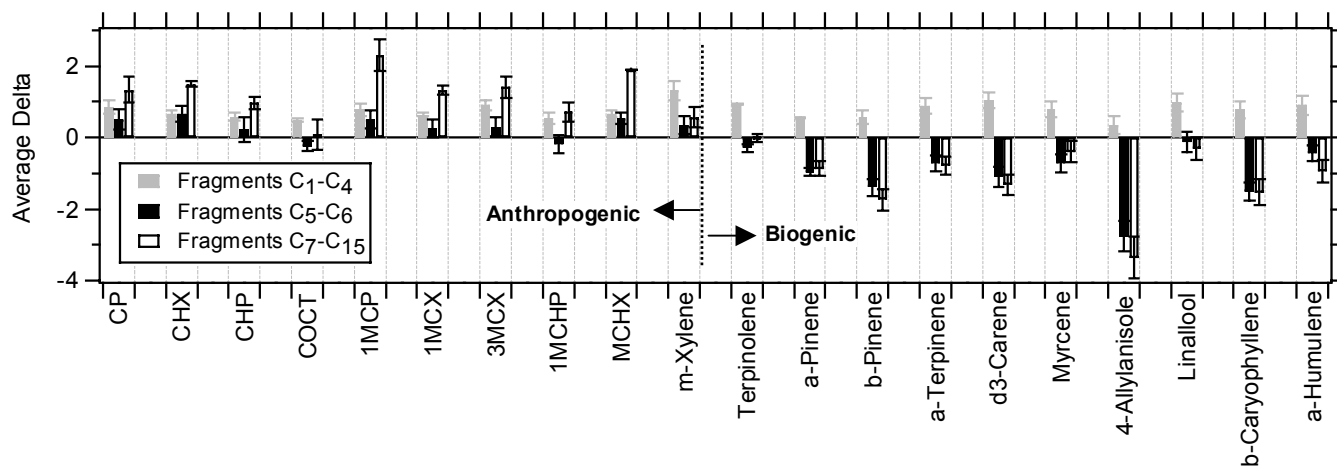


Figure 10.10. Relative contribution of higher molecular weight fragments to total organic mass during ozonolysis of α -pinene in the presence of different seed particles. Increased fraction of larger fragments to SOA formed during acidic MgSO_4 experiment indicates greater extent of acid-catalyzed reactions that form higher molecular weight species.

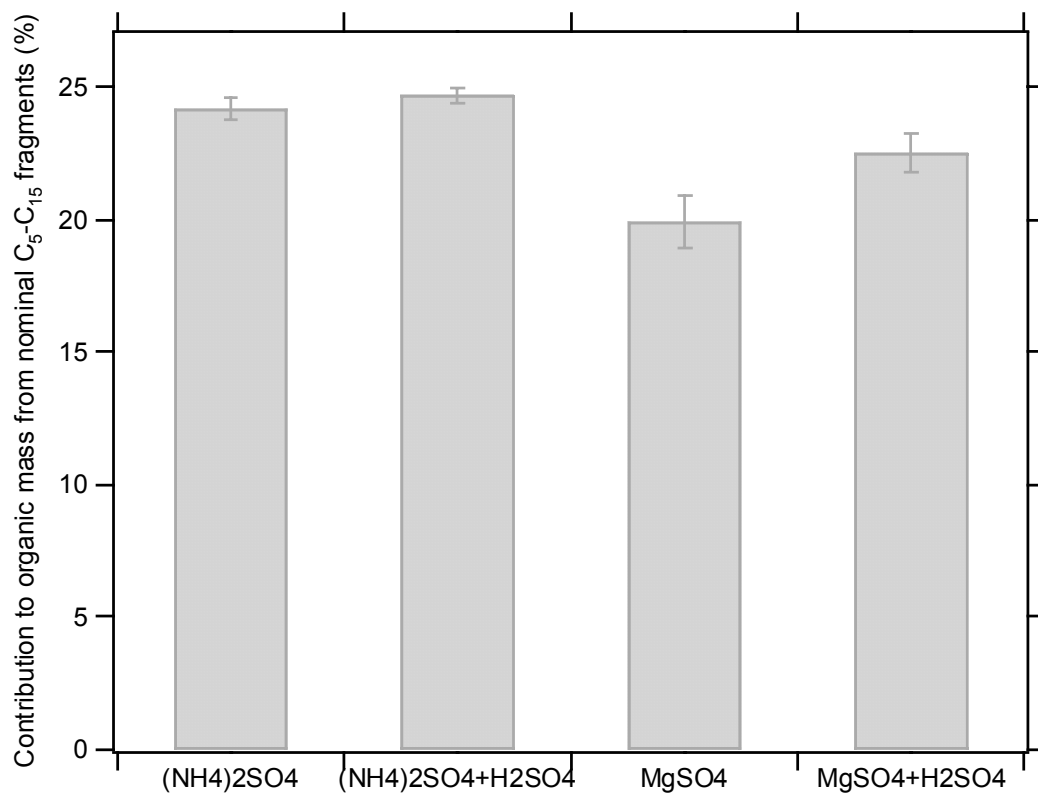
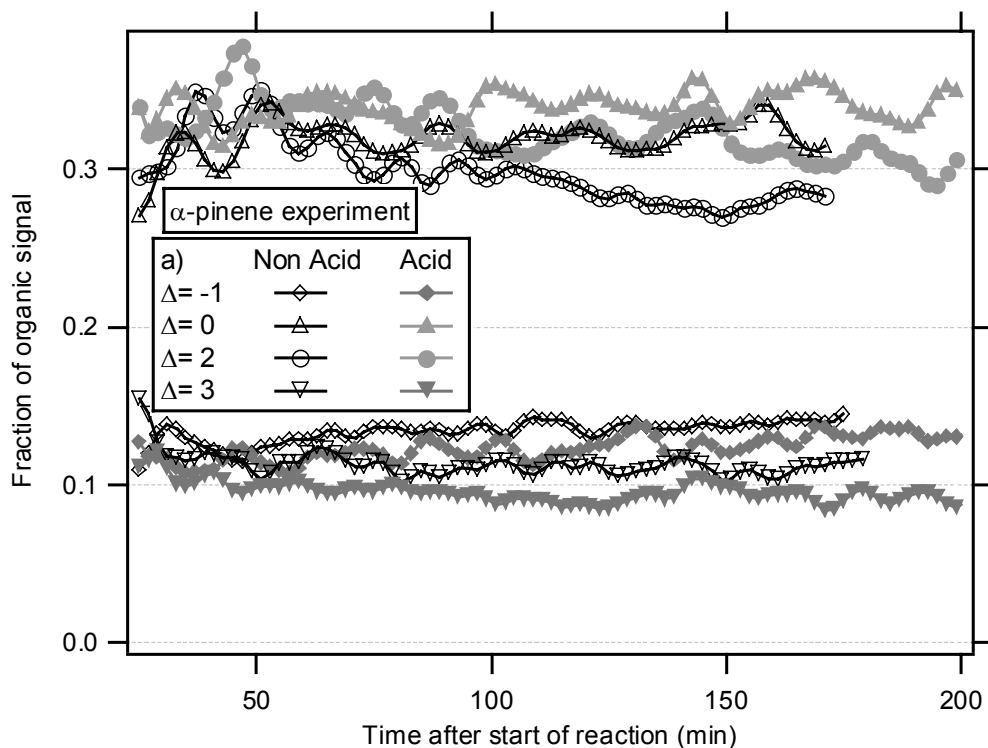


Figure 10.11. (a) Relative contribution of different Δ groups to total SOA mass formed from ozonolysis of α -pinene in the presence of MgSO_4 or $\text{MgSO}_4+\text{H}_2\text{SO}_4$ seed aerosols. (b) Fraction of organic signal due to m/z 44 and $\Delta=3$ during ozonolysis of α -pinene in the presence of MgSO_4 or $\text{MgSO}_4+\text{H}_2\text{SO}_4$ seed. Increased contribution of $\Delta = -1$ and $\Delta = 0$ and decreased contribution of $\Delta = 3$ (or m/z 44) to total mass during acid experiment are consistent with acid-catalyzed reactions.



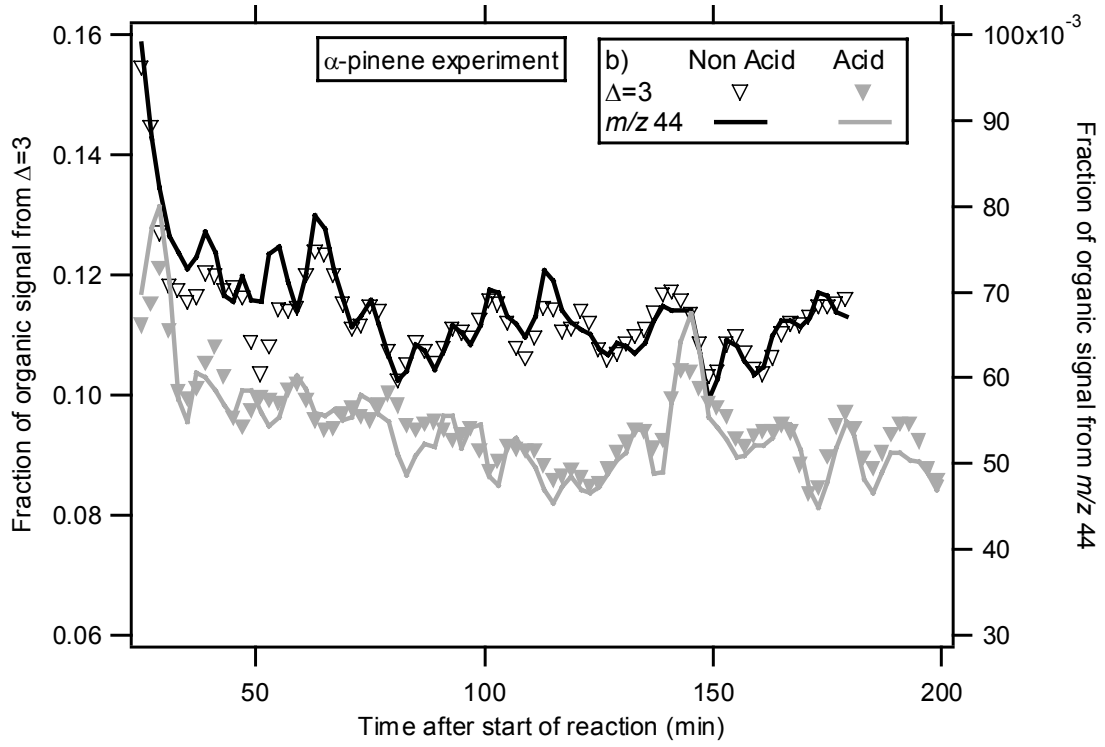
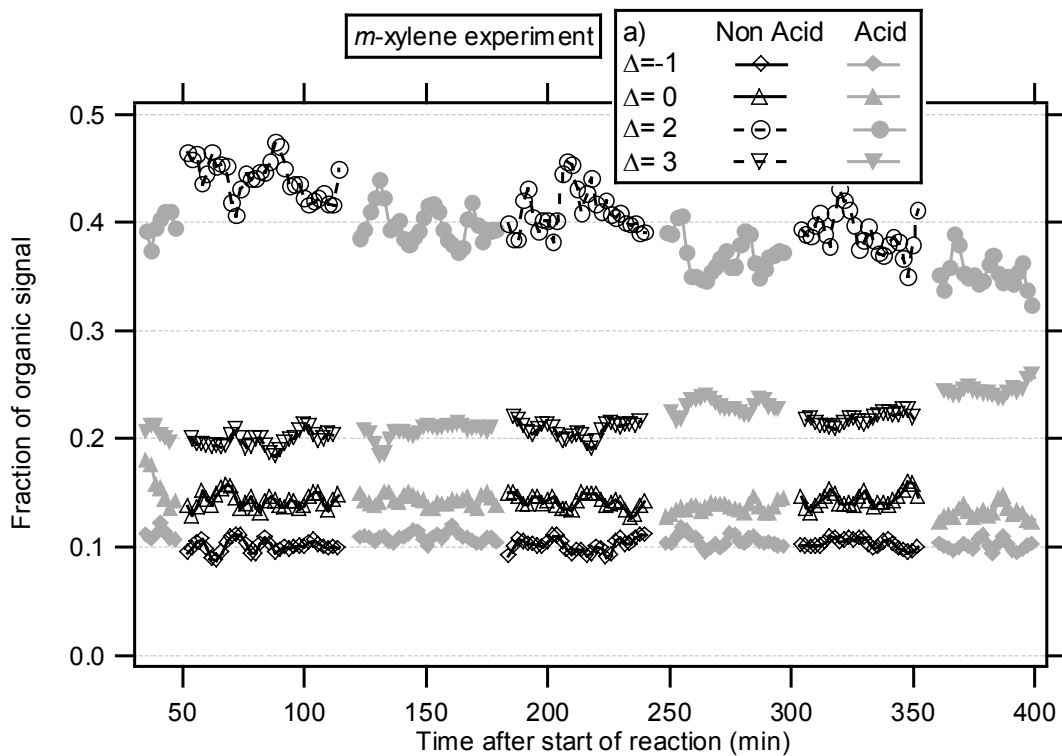


Figure 10.12. (a) Relative contribution of different Δ groups to total SOA mass formed from photooxidation of *m*-xylene in the presence of $(\text{NH}_4)_2\text{SO}_4$ or $(\text{NH}_4)_2\text{SO}_4 + \text{H}_2\text{SO}_4$ seed aerosols. (b) Fraction of organic signal due to m/z 44 and $\Delta=3$ during photooxidation of *m*-xylene in the presence of $(\text{NH}_4)_2\text{SO}_4$ or $(\text{NH}_4)_2\text{SO}_4 + \text{H}_2\text{SO}_4$ seed aerosols. Increased contribution of $\Delta = 3$ to total signal correlates well with increased contribution of CO_2^+ fragment of oxygenated organics (m/z 44).



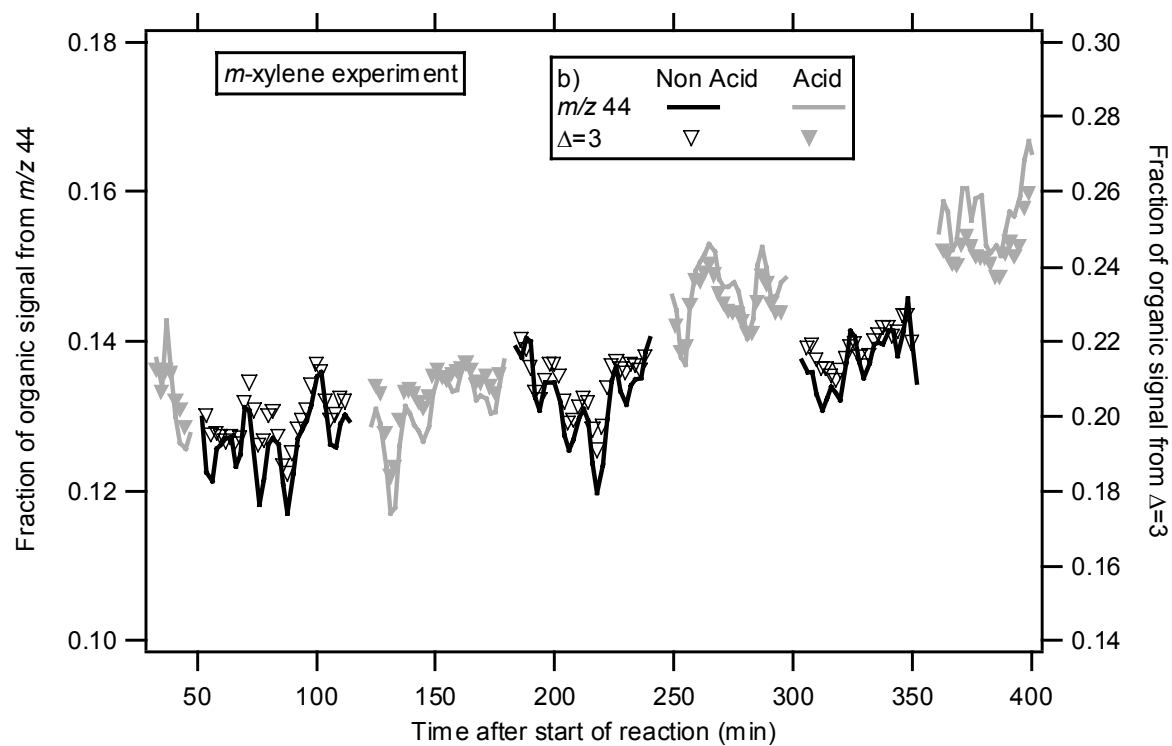


Figure 10.13. Time trend of main fragments of 2,5-furandione (m/z 54), 3-methyl-2,5-furandione (m/z 68), and nitrate (m/z 30 and 46) during photooxidation of *m*-xylene. Increase in the intensity of these fragments after start of reaction is consistent with presence of furandione compounds and nitro-compounds in SOA.

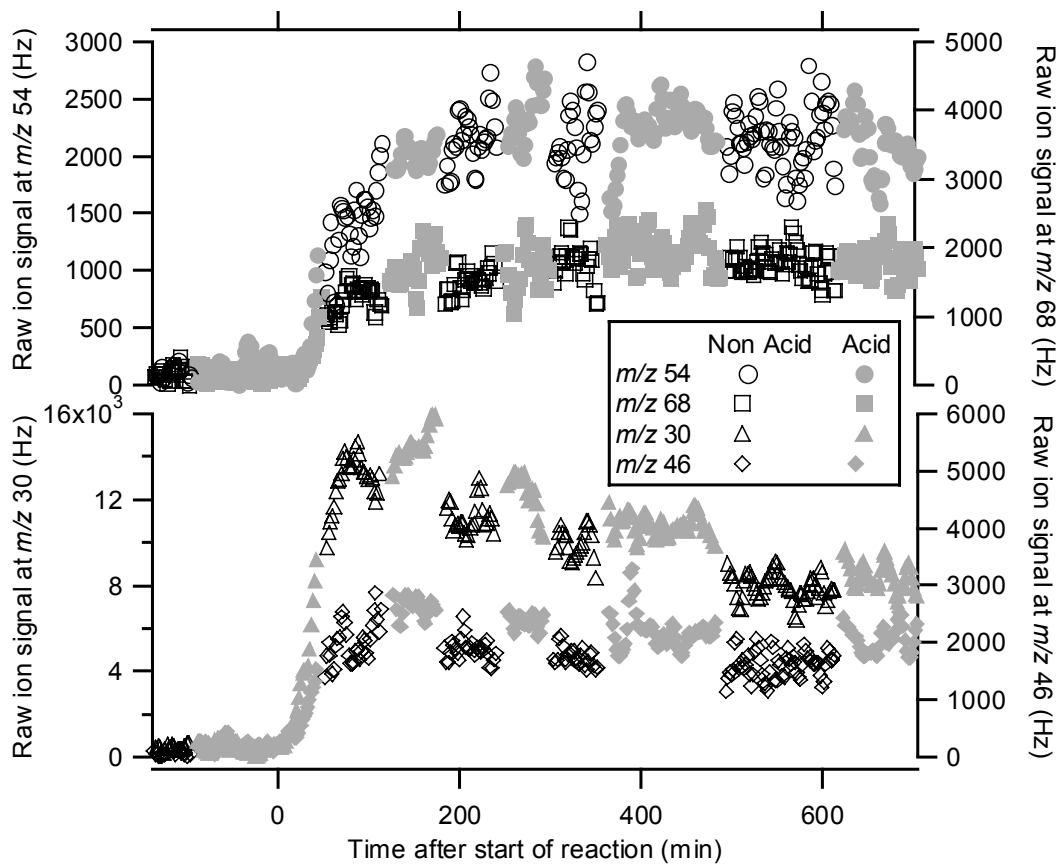


Figure 10.14. Mass spectra of SOA formed during α -pinene, *m*-xylene, and cyclopentene oxidation experiments as well as ambient organic mass spectra of Ohio background pollution, Cleveland, OH pollution, and brush fire plumes. Common dominant fragments at m/z 41, 43, 44, and 55 are observed in all mass spectra.

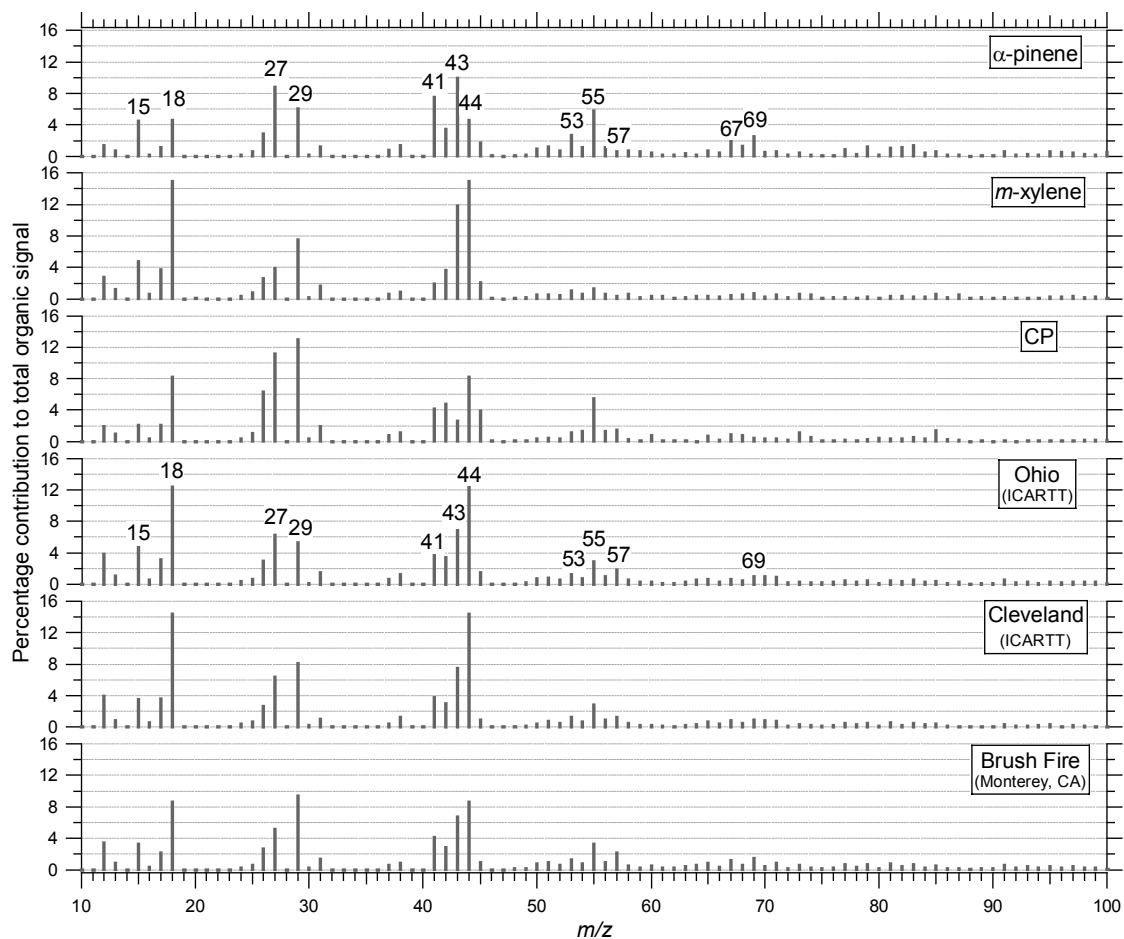
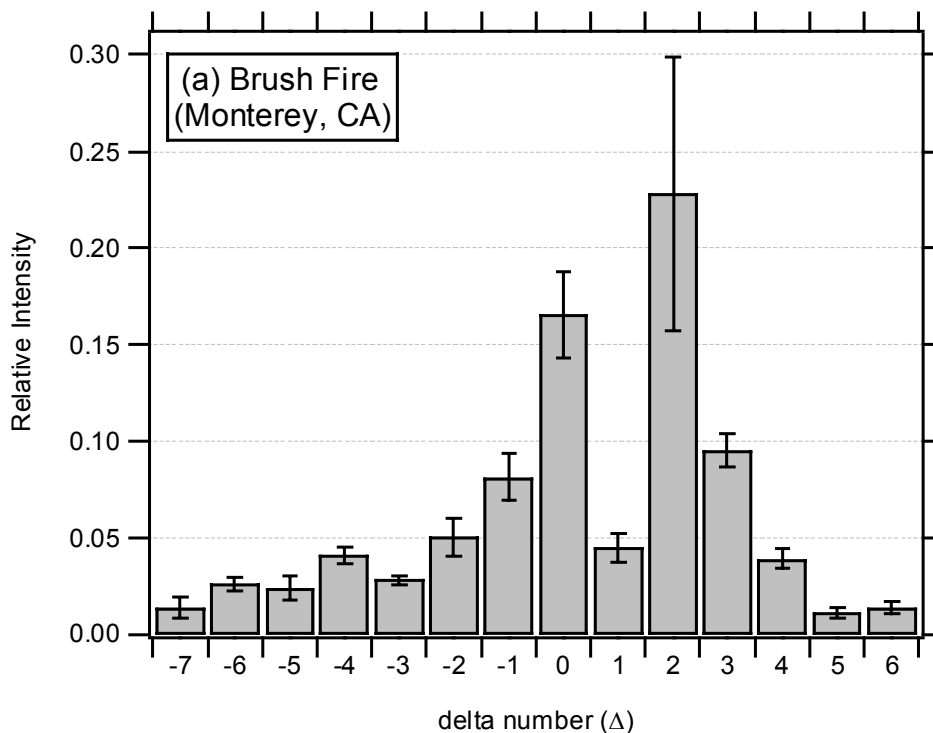


Figure 10.15. Delta analysis of mass spectra obtained from brush fire, Cleveland, and background Ohio pollution plumes. Organic composition in all these air masses is very similar and dominated by fragments with $\Delta=2, 0,$ and 3 . In cases when similar air masses were sampled in more than one occasion, the error bars represent the standard deviation of the average to indicate the extent of variation in the averaged delta values.



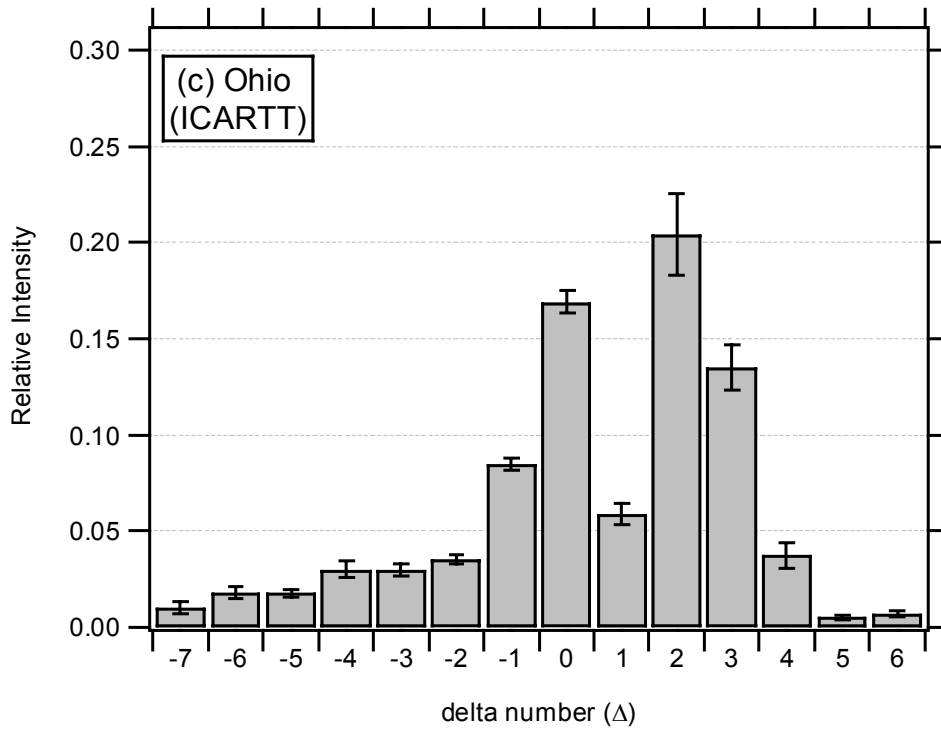
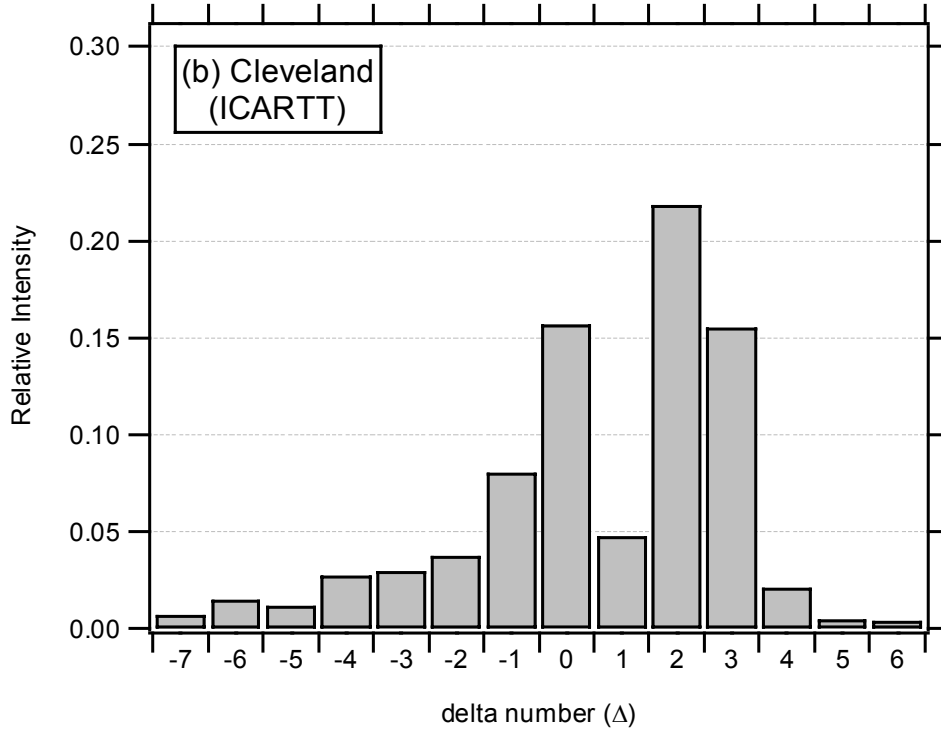


Figure 10.16. Average delta values of different size fragments of ambient organic mass spectra obtained in brush fire, Cleveland pollution, and background Ohio pollution plumes. Larger fragments in these mass spectra exhibit negative delta values. The error bars represent the standard deviation of the averaged delta values in each category.

